DTU Civil Engineering
Department of Civil Engineering

ARCTIC TECHNOLOGY CENTRE

Master Thesis

Determining Snow Depth Distribution from Unmanned Aerial Vehicles and Digital Photogrammetry

Technical University of Denmark (DTU), Spring 2015

Author:

Emiliano Cimoli, s131393

Supervisors:

Carl Egede Bøggild

Fred Sigernes

Co-supervisor:

Sebastian Bjerregaard Simonsen

Determining Snow Depth Distribution from Unmanned Aerial Vehicle and Digital Photogrammetry

Author

Emiliano Cimoli

M.Sc. Student in Environmental Engineering

DTU Environment

Emicimoli@hotmail.com

+45 60 52 55 12

Grøntoften 8 st. tv.

2870 Dyssegård, Denmark

Supervisors

Carl Egede Bøggild

Danmarks Tekniske Universitet

cebo@byg.dtu.dk

+45 25 22 27

Brovej

Bygning 118, rum 163

2800 Kgs. Lyngby, Denmark

Fred Sigernes

The University Centre in Svalbard

fred.sigernes@unis.no

+47 79 02 33 35

Pb. 156, 9171 Longyearbyen, Norway

Co-supervisor

Sebastian Bjerregaard Simonsen

Danmarks Tekniske Universitet

ssim@space.dtu.dk

+45 25 97 74

Elektrovej

Bygning 327, rum 011

2800 Kgs. Lyngby, Denmark

PREFACE

The present master thesis constitutes 30 ECTS and is presented to DTU Byg and DTU Artek as a final project for the completion of a MSc in Environmental Engineering at the Technical University of Denmark.

The project was carried on in collaboration with the University Center in Svalbard (UNIS) and was funded by the Arctic Field Grant (AFG), Grønlandsbanken and the Society for Arctic Research and Technology (SAFT). The Svalbard fieldwork campaigns were funded by the AFG meanwhile the Greenland fieldwork campaigns where funded by Grønlandsbanken and SAFT. I express my deepest gratitude to these institutions for lending me the opportunity to work on such a fascinating project that I strongly aspired to carry on.

This study constitutes a component of a wider project carried on in collaboration with Marco Marcer and Baptiste Vandecrux under the supervision of Carl Egede Bøggild from DTU Artek and Fred Sigernes from UNIS.

Knowing that snow cover is the dominant surface in the Arctic and has extremely important influence in the livelihood and well-being of its residents, this wider project was born with the idea of providing new and efficient tools for monitoring snow through the use of the recently emerging Unmanned Aerial Vehicles (UAVs) platforms.

Overall the project is divided in three components that are enlisted as follows.

- Designing and testing a new and affordable method for determining snow depth distribution using UAVs and digital photogrammetry.
- Using snow depth UAV data for calibrating models that can estimate snow depth distribution over large scale areas.
- Using the UAV acquired imagery for obtaining further information of snow optical proprieties and link them with the physical proprieties.

The present master thesis covers the first component of the project and focus on the use of UAVs combined with digital photogrammetry for estimating snow depth spatial distribution.

The second and third part of the project are covered by Marco Marcer and Baptiste Vandecrux on their master thesis work. Since this project was carried on simultaneously with Marco and Baptiste project, the UAV data for snow distribution modeling was not yet available for the second component. However, the overall project is still in progress and further studies are to be followed.

ACKNOWLEDGMENTS

I would like to express my most sincere gratitude to my supervisor Carl Egede Bøggild for making all this possible in the first place. During the fieldwork campaigns his teachings were more than purely academic, and without his support this project would not have even started.

I am extremely grateful to Sebastian Bjerregaard Simonsen for his interest and support on the project and all the wise advices he provided during the course of it (And for lending C3Po).

My greatest thanks goes also to Fred Sigernes and Chris Borstad for their huge support on the Svalbard campaigns and their precious advices.

Special thanks as well to Martin Kotol for his support in the Greenland summer campaign, the good time spent together and from rescuing from critical situations.

My deepest gratitude goes to my fellow pilots Timon Brüggemann and Marius Petersen from whose I still have so much to learn.

A lot of thanks also to Inger Lill Bratbergsengen for his kindness and assistance and providing crucial parts for the project.

Thanks to all the Artek and UNIS staff for being so nice, helpful and shiny even in the gloomiest Arctic days.

Infinite thanks to my family that was always supporting, and to Mario for always backing me up with his drone army.

To all my friends and to Veronica Cuttone that were always there in the moments of intense tachenza.

Thanks to my Walkera X350 Pro (R.I.P.), that considering his nature, it battled gloriously in the difficulties of the Arctic.

Finally, I would like to give the most special thanks to my friends, flatmates, colleagues and “brothers in arms” in this big project and adventure Marco Marcer and Baptiste Vandecrux. Thanks for all the cigars smoked together, the countless GCPs moved in harsh environments and their creativity for cooking fiskeboller.

“Sic Parvis Magna”
("Thus great things from small things -come-")

-Sir Francis Drake motto

ABSTRACT

Determining snow depth spatial distribution is crucial not only for serving civil purposes related to drinking water supply or hydropower generation, but also for several applications in snow, hydrology and environmental research. However, snow depth results to be extremely variable both in space and time. Consequently, traditional and state-of-the-art snow monitoring methodologies are not always able to capture such a high spatial variability over time without highly expensive solutions. In the present work a new methodology is presented that aims to propose a solution to the problem by taking advantage of two low-cost and emerging technologies in a geoscience research context; Structure from Motion (SfM) digital photogrammetry and Unmanned Aerial Vehicles (UAVs). The asset of the combination between these technologies is that they can provide accurate and high resolution Digital Elevation Models (DEMs) of large areas, at low-running costs and at a reduced effort. The proposed method would profit of this asset and perform a subtraction between georeferenced snow surfaces (snow DEMs) and their corresponding underlying topographies (topography DEMs), thus providing snow depth distribution maps. In order to test the feasibility and efficiency of the presented method on a small scale level, six different snow covered areas were surveyed in the mentioned above context. The areas ranged from 900 to 51,000 m^2 and two were located near Longyearbyen, Svalbard and four near Andenfjorden, West Greenland. The surveys differed in terms of snow surface type, underlying topography complexity, luminance conditions and equipment used in order to assess an applicability range for the method. The results are presented as six snow depth distribution maps and are validated by comparing estimated snow depths to probed snow depths over a set quality control points. Depending on the area, the average difference between probed and estimated snow depth varied from 0.01 m for the best case to 0.19 m for the worst case, meanwhile the spatial resolution ranged from 0.06 to 0.1 m. The error sources for each case are thoroughly investigated and it was assessed that the error can be further mitigated by georeferencing the DEMs using common ground control points visible in both the snow surface and the corresponding underlying topography. In the tests performed, the method did not result particularly limited by any specific surface characterization of the area or any survey condition. Even though it was tested over small scale areas, by considering these preliminary results the method presents the potential to be a simplified procedure that allows repeat-mapping of snow dynamics while mitigating running costs and without resigning at obtaining high accuracies and resolutions.

CONTENTS

1 INTRODUCTION

Snow cover is an extremely dynamic surface that is continuously varying over space and time (Robinson, et al., 1993; Dèry & Brown, 2007; Scipiòn, et al., 2013), and this variability has a critical role in climate, ecological and hydrological systems both on a local and on a global scale (Winther, et al., 2003; Callaghan, et al., 2011; UNEP, 2007). Fom an hydrological point of view, the volume of water in the snow or Snow Water Equivalent (SWE), is the most important propriety of the snow cover and is directly related to the snow depth (*HS*). In this context, is extremely desirable to estimate snow depth distribution and variability since it results a key component in snowmelt-runoff modeling (e.g. Butt & Bilal, 2011), in river run-off and groundwater recharge (e.g. Akyürek & Şorman, 2002; Jain, et al., 2008) and as a fundamental direct resource indicator for fresh water supply or hydropower generation (Barnett, et al., 2005). For society the snow depth variability is also important, when estimating hazards in the case of avalanches and floods (e.g. Schweizer, et al., 2008; Jamieson & Stethem, 2002) or for example it has been observed that it has an impact on vegetation growth on certain types of land cover (Wanga, et al., 2013; Peng, et al., 2010). It is foreseen the need to efficiently and accurately estimate snow distribution over time for improving several environmental research sectors, but also for increasing the efficiency of water resources management systems. Furthermore, it is here noted that this need is accentuated in Arctic and Nordic regions, where snow is the dominant surface covering both its land and frozen water bodies for 8-10 months each year and the use of snow as a hydropower or water supply resource is particularly exerted (Winther, et al., 2003; Callaghan, et al., 2011; Vikhamar & Solberg, 2003).

However, despite its relevance, traditional and state-of-the-art methods for estimating snow depth present some serious drawbacks and limitations. Manual snow probing is the simplest technique available, but this method is time consuming, presents very low spatial coverage and cannot be practiced in hazardous environments like avalanche risk zones (Prokop, et al., 2008). Time consuming issues are solved by the implementation of automated snow depth point measurements like snow pillows or sonic rangers but the spatial coverage of these methods still remains very poor (e.g. Liston & Sturm, 2002; Serreze, et al., 1999; Slater & Clark, 2006). The Ground Penetrating Radar (GPR) provides an accurate extra spatial coverage but it remains very discrete in terms of spatial variability and can't be practiced over dangerous areas without expensive airborne approaches (Machguth, et al., 2006)

Remote sensing methods for determining snow depth usually fills the gap in regards of spatial coverage compared to the other methodologies. Several comparisons among them have been performed and an extensive review on the topic has already been done (Dietz, et al., 2011). Among these methods one can mention the use of satellite platforms and microwave emissivity (e.g. Rott, et al., 2008; Clifford, 2010; Rittger, et al., 2013; Parajka & Blöschl, 2008), airborne or terrestrial Light Detection and Ranging (LiDAR) (e.g. Deems, et al., 2013; Hopkinson, et al., 2004; Prokop, 2008) and traditional airborne photogrammetry (König & Sturm, 1998; Worby, et al., 2008). Even though these are established techniques they often present some limitations in accuracy and resolution, in the ease of application or either they come at high costs (Clifford, 2010; Rittger, et al., 2013; Rott, et al., 2008; Parajka & Blöschl, 2008; McKay, 1968; Al-Wassai & Kalyankar, 2013; Xhardè, et al., 2006).

Likewise, various current modeling approaches, either statistical or physically based, are able to provide snow depth and SWE over small local areas or catchment scale areas (e.g. Bruland, et al., 2004; Grünewald,

et al., 2010; Grünewald, et al., 2013). Yet, these tools not always provide the needed accuracy and require a significant amount of input data together with elevated computational costs (Bavera, et al., 2014).

This thesis investigates a new alternative method for estimating snow depth spatial distribution by combining two emerging technologies in the geosciences research sectors which are Structure from Motion (SfM) digital photogrammetry and the use of Unmanned Aerial Vehicles (UAVs). SfM is able to reconstruct 3D models of terrain surfaces from a set of overlapping pictures of the terrain itself. These pictures are afterwards georeferenced using points of known global coordinates visible in the overlapping images, thus providing Digital Elevation Models (DEMs) of the terrain topography (Westoby, et al., 2012; Fonstad, et al., 2013; Cimoli & Marcer, 2014). UAVs are small remotely controlled flying platforms capable of carrying limited payloads e.g. cameras. They have already been successfully applied together with SfM for this purpose due to the optimal camera perspective perpendicular to the ground they can provide. These are characterized by being able to cover large areas with the minimum effort involved (Lucieer, et al., 2012). Their combination not only has been shown to produce very accurate results but the equipment needed to apply these techniques is purchasable at a consumer grade level since only a camera and an UAV platform are required (Dowling & Gallant, 2013; Harwin & Lucieer, 2012; Colomina & Molina, 2014).

The new proposed method takes advantage of SfM using UAV acquired imagery and then simply subtract the georeferenced snow surfaces (snow DEMs) and the underlying snow free georeferenced topographies (terrain DEMs). Even tough similar approaches have been very recently investigated (Bühler, et al., in press; Nolan, et al., 2015), they involve the use of expensive scanners and manned airborne solutions. Instead the present method would provide a cheaper, easily adoptable and accurate alternative for estimating snow depths without giving up on spatial resolution.

However, reconstructing snow surfaces using SfM is unprecedented and is considered problematic due to the non-heterogenic texture and the lack of features that the photogrammetric tool requires for generating the 3D models (Westoby, et al., 2012; Fonstad, et al., 2013). This issue could be accentuated in some Arctic regions where several days are characterized by frequent overcast days. These conditions causes low luminance which is the element that defines the amount of highlights, shadows and contrast present in a photograph; with no luminance, there would be no shadows and no contrast, and thus there would be no patterns and details in a photograph which are mandatory for the SfM reconstruction (Jacobson, et al., 2000; Ballabeni, et al., 2015).

In order to verify the feasibility and efficiency of the proposed method in the above mentioned context, a total of six different relatively small snow covered areas where mapped during April 2015 in two different Arctic regions. Two areas were mapped in Breinosa near Longyearbyen, Central Svalbard and four near Andenfjorden close to Sisimiut, West Greenland. Mapping of the same six areas was afterwards performed during July 2015 when almost all the terrains were completely snow free. During the course of these campaigns various kinds of snow surfaces and topographies where mapped under different luminance conditions and camera settings. These tests were done in order to try to push this new method to its limits over small scale areas and thus being able to assess an applicability range for future realistic case scenarios. In this work the word mapping is interchangeably used to identify the process of DEM generation from an UAV survey. However, the term still differs from the more specific snow depth mapping.

1.1 PROJECT GOAL AND MOTIVATION

The objective of this project can be stated in one sentence as follows:

"To design, validate and report a new methodology for estimating high accuracy and high resolution snow depth distribution maps by utilizing modern and more accessible technologies compared to other conventional and state-of the-art methods."

Besides, considering the difficulties of using SfM for mapping featureless surfaces like snow, the present work intends to overcome this issue by testing its feasibility using the UAV platforms and to improve the reconstruction performances by means of easily applicable batch image processing.

Considering the rapid variability of the snowpack over time, is clear the importance of having a low-cost method that still provide precise results. As previously mentioned in the introduction, this methodology could result useful for a variety of research fields and civil purposes. However, it could result particularly useful for hydropower companies in Arctic or Nordic countries like Norway where 99% of the electricity is produced from hydropower or Switzerland with a 60% (Vikhamar & Solberg, 2003). For example, in Norway, the value of the snow storage is approximately 4 billion US dollars in an average year, and hence small errors in the estimation of this storage represent large values (Bruland, et al., 2015). For Arctic and Alpine regions it could also be extremely helpful for estimating snow depth in avalanche risk areas and eventually predict its possible occurrence by remotely maneuvering the UAV over the hazardous area from a safe location.

It has to be mentioned that the current thesis project tests the proposed method on significantly small areas compared to catchment scale areas within the range of 900 to 51,000 m^2. Nevertheless, the work aims to scientifically test the feasibility of the photogrammetric method as a first step for future commercial solutions.

1.2 THESIS OUTLINE

After having provided the background of the thesis research area, the thesis provide an insight on the basic concepts behind the application of the method in Chapter 2. In Chapter 3 all the six studied areas are enlisted and described in terms of surveying conditions and terrain characteristics. Chapter 4 describes step-by-step the design and application of the fieldwork component of the method. In Chapter 5 the procedures applied for processing the acquired fieldwork data are described. Chapter 6 shows the results obtained in this first iteration of the method and points out the main discoveries. Chapter 7 takes a particular and unusual form; it summarizes what was done and inquires about the outcomes of this work and addressing the weaknesses of the method for a future real applicability. Finally, Chapter 8 outlines the direction of future work and research. All chapters end with a conclusion note pointing out the key points and findings.

2 BACKGROUND THEORY

In the following chapter the basic theory and concepts behind this new method are briefly covered. The chapter starts by illustrating the basic snow proprieties closely related to the method focus and is followed by illustrating the fundamental principles involved for understanding it. Background theory of SfM and UAV mapping is given with a geosciences focus due to the vast range of applications these technologies have. Elements of digital image processing where omitted in order to avoid overloading the report, however main concepts are explained along the way of the thesis.

2.1 SNOW PROPRIETIES: DEPTH, DENSITY AND SNOW WATER EQUIVALENT (SWE)

As mentioned in the introduction, seasonal snow cover is the most transient element of the whole earth surface due to its extreme variability in space and time. Approximately 30 million km^2 are covered with 0.1 to 4 meters of snow each winter in the Northern Hemisphere (Fohn, 1989; Lemke, et al., 2007; Dèry & Brown, 2007; Robinson, et al., 1993) and snow can persist on one specific location from the short time of a few days to a major portion of the year (Street & Melnikov, 1990). These spatial and temporal fluctuations arise in response to the different microclimates and terrains topographies of the specific area experiencing seasonal snow cover (Street & Melnikov, 1990)

The snow deposited on the ground or the commonly called snowpack is characterized by many particular features. Among them we have textural and stratigraphic characteristics, crystal morphology like snow grain size and shape, snow density and hardness, snow temperatures and liquid water content or SWE. A description of all these features goes out of the scope of the thesis, however it is provided by international standards in The International Classification for Seasonal Snow on the Ground together with the standard scientific measurement procedures (Fierz, et al., 2009). The current chapter will focus on the description of the snow depth, density and water equivalent since are central snow proprieties in the context of the new method presented in this thesis work.

Snow depth (HS) Referred as the vertical distance from a relative terrain base (H_g) to the snow surface (H_s) (cm) as depicted in Eq. 1. Is related to a single location at a given time and is traditionally measured with a snow probe or snow stakes.

$$HS = H_s - H_g \qquad (1)$$

Is extremely variable in space and this spatial heterogeneity is ruled by several factors like the elevation that defines the snow-rain transition (e.g. Grünewald, et al., 2014; Avanzi, et al., 2014; Klos, et al., 2014), the terrain topography (e.g. Lehning, et al., 2008), the shadows and aspects of the local terrain influencing the snow melting rates (e.g. Marsh, et al., 2012), the wind redistribution causing snow drift (e.g. Lehning, et al., 2008) and the surface vegetation type (Elder, et al., 1991; Ellis, et al., 2010).

Snow density (ρ_s) Defined as the mass of snow per unit volume $(\mathrm{g\,cm^{-3}})$ and considered as a bulk propriety for the majority of applications. Is normally measured by weighting snow of a known volume and its estimation requires significant more effort than estimating snow depth. Densification of the snowpack is mainly caused by wind erosion, melt-refreeze events, compaction and snow metamorphism (Sommerfeld & Lachapelle, 1970; Colbeck, 1982).

Snow Water Equivalent (*SWE*) The SWE is the depth of water that would result if the mass of snow melted completely (cm). Obtaining SWE is the main goal due to its relevance for hydrological purposes. SWE is the product of the HS and the vertically-integrated density. At a given point is calculated with Eq. 2.

$$SWE = HS \times \frac{\rho_s}{\rho_w} \quad (2)$$

Where ρ_s is the bulk density ($\mathrm{g\ cm^{-3}}$), ρ_w the density of the water ($1\ \mathrm{g\ cm^{-3}}$) and HS the snow depth (cm).

Measuring ρ_s on one point involves much more effort when compared to a measure of the *HS* at the same point (López-Moreno, et al., 2013), therefore due to their importance several studies and investigations have been proposed that are able to efficiently estimate spatially distributed ρ_s from HS data in order to calculate the SWE thus minimizing the efforts (Sturm, et al., 2010; Jonas, et al., 2009; Bormann, et al., 2013; Bruland, et al., 2015; McCreight & Small, 2014). Nonetheless, since the spatial variability of ρ_s is considerably smaller than the one of *HS* (Sturm, et al., 2010), a simpler and usually practiced technique is to measure density over one specific point and consider it representative of the whole area. It can be said that considering the tools available for estimating ρ_s, the main interest lays on accurately acquiring snow depth with high spatial resolution.

2.2 Elements of Digital Elevation Models (DEMs) and Global Navigation Satellite Systems (GNSS)

A digital elevation model (DEM) can be defined as "any digital representation of the continuous variation of relief over space" (Burrough & McDonnell, 1998). A DEM usually consists of a gridded matrix that represents elevations of an area of the earth's surface. These datasets are very valuable for resource-related Geographic Information Systems (GIS), hydrological modelling purposes or environmental change applications to mention a few.

Various methodologies exists for extracting DEMs and they can provide a wide range of resolutions, from centimeter to the order of dozens of meters. Their quality is usually measured from their resolution (or cellsize) and their vertical accuracy. Even though they can result very accurate and are accepted as true representations of the earth surface they are always subject to errors (Wechsler & Kroll, 2006; Wechsler, 2007). One way to quantify the accuracy is in the form of Root Mean Square Error (RMSE) statistics by comparing the DEM with some specific points that are considered as true representative of the actual position in a geographic coordinate system. The RMSE expression is shown in Eq. 3.

$$RMSE = \sqrt{\frac{1}{n}\sum_{i=1}^{n} \Delta h_i^2} \quad (3)$$

Where Δh_i is the difference in position or elevation between the "true" precisely measured point and the corresponding point in the DEM and *n* is the number of comparison test points.

The RMSE is basically a standard deviation and is therefore grounded on the assumption that these errors present in the DEM are random and normally distributed. The RMSE is widely used to establish DEMs accuracy (Wechsler, 2007), but to ensure the RMSE to representative as DEM error GCPs needs to be well-distributed over the study area. When utilizing DEMs for a particular application, errors rooted in the DEM

might affect the application itself. Thus, other methods for a more accurate evaluation of these uncertainties have been proposed (Wechsler & Kroll, 2006; Wechsler, 2007).

Geographic coordinate systems or geographic reference systems (CSR) are systems for precisely specifying any location on earth with a set of numbers or letters (Uren & Price, 2010). Every DEM is referenced according to real world coordinates specified by a CSR. Several techniques exists for obtaining the elevation data and for assigning it to real world coordinates (Li, et al., 2005). Most modern techniques involves the generation of accurate digital representations of the earth surface through the use of different kinds sensors or photogrammetry and the assignation of known points in the digital representation with real world coordinates that are acquired via Global Navigation Satellite Systems (GNSS).

These systems consists of Earth-orbiting satellites that broadcast their locations in space and time, of networks of ground reference stations and of receivers that calculate positions of ground points by trilateration (U.N. Office for Outer Space Affairs, 2012). The Global Positioning System (GPS) is a specific fully operational GNSS among others like the GLONASS or Galileo, and is the most commonly used. Depending on the precision desired, the time invested and the ease of data processing distinct devices and survey types exists for determining coordinates of the desired ground positions. A professional GNSS device consists of an antenna for receiving satellite data and a receiver for storing the data. When an antenna and a receiver are being positioned around acquiring points the device is also termed rover.

An important concept that plays a major role in this thesis is Differential GNSS (DGNSS) positioning which enhances the used GNSS system by correcting the pseudoranges of the receiver (Figure 1). The pseudoranges are the *pseudo* distances from the receiver to the satellites (Ghilani & Wolf, 2012).

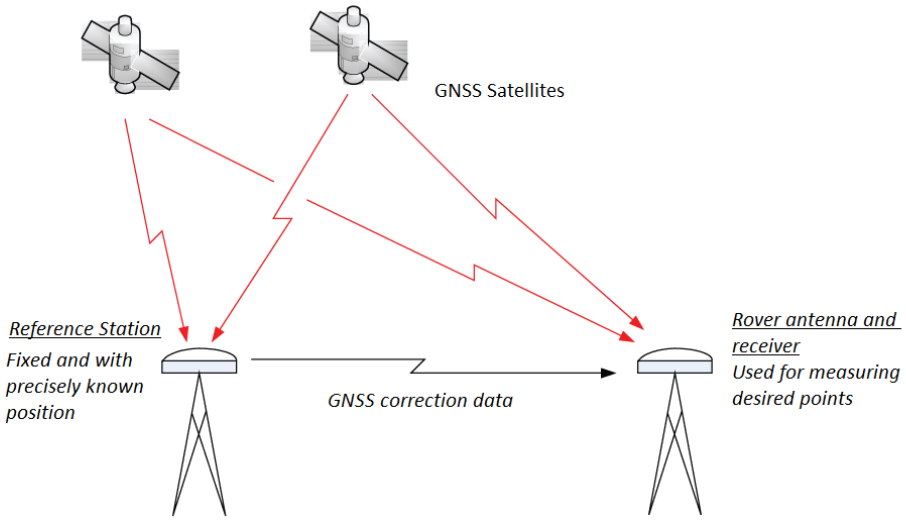

Figure 1: *The DGNSS concept illustrated. Calculated correction data from a reference station is used to correct the pseudo distance error and provide a better positioning estimate.*

These errors in the distance estimation are caused by the satellite atomic clock precision, by satellite drifts from its orbit and also from the signal delay when it passes through the atmosphere. The DGNSS process corrects these *pseudoranges* through the use of nearby reference stations whose position is almost exactly known. By knowing the almost exact position of a nearby reference stations (or baselines) that are

continuously observing is possible to calculate the error on the measured distance. This error is afterwards subtracted to the nearby acquired points. DGNSS process can be done in post-processing after having acquired the desired points and can achieve very high accuracies in the order of centimeters or millimeters depending on the time invested in the survey.

2.3 Structure from Motion (SfM) Digital Photogrammetry Applied to Geosciences

The SfM methodology is basically able to reconstruct 3D models of objects or scenes from a set of overlapping pictures of the feature itself taken from a normal camera. The method has several uses across various disciplines, however the focus will be given in the context of the thesis. A refined introduction and pipeline to the method has already been done in previous work (Cimoli & Marcer, 2014). The process differs from traditional photogrammetry since the geometry of the scene, the camera positions respective to the object and the orientation are solved automatically without needing a network of targets with known local 3D positions (Figure 2).

SfM instead solves the problem simultaneously through a highly redundant, iterative bundle adjustment procedure based on a database of features automatically extracted from a set of multiple overlapping images (Snavely, 2008).

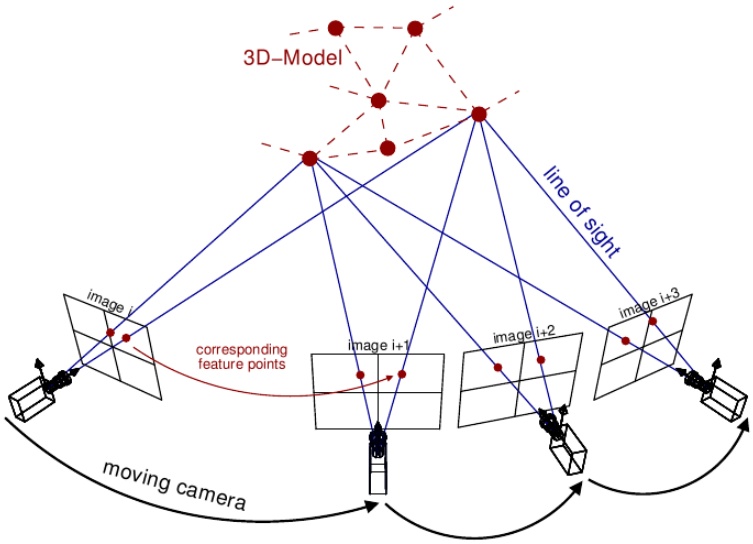

Figure 2: The SfM concept; 3D models are reconstructed from a set of overlapping pictures by using feature recognition.

Indeed, the overall SfM process goes through a set of computer vision algorithms that are very briefly commented in the following four steps. Initially a feature tracking algorithm like the Scale Invariant Feature Transformation (SIFT) detector is used to identify patterns or "descriptors" across the set of pictures (Lowe, 2004).

This first step is extremely important since the object reconstruction heavily relies on the presence identifiable features represented by a set of pixels among the pictures; this is why highly textureless

surfaces like snow or sand present reconstruction difficulties (Westoby, et al., 2012; Fonstad, et al., 2013; Furukawa, et al., 2004). Afterwards the camera external and internal parameters are solved by a bundle adjustment algorithm (Triggs, et al., 1999) providing a sparse point cloud representing the scene. The density of this point cloud is then highly augmented by implementing Clustering View for Multi-view Stereo (CMVS) and Patch-Based Multi-view Stereo (PMVS2) (Furukawa & Ponce, 2007; Furukawa, et al., 2010). Finally, a fit 3D mesh is produced from the dense point cloud using traditional interpolation methods, usually triangulation. Is noticed this last step how the amount of matched and cloud points are an indicator of how well the object is being reconstructed. Performing a deeper overview of the computational methods of SfM goes out of the scope of the thesis. However, more detailed investigations and reviews on the topic are available in literature (Westoby, et al., 2012; Remondino & El-Hakim, 2006).

SfM has already been addressed as an efficient, accurate and low cost tool for geoscience applications by being able to generate high precision DEMs compared to other established methods like terrestrial or airborne LiDAR and Interferometric Synthetic Aperture Radar (IFSAR) sensors (Westoby, et al., 2012; James & Robson, 2012; Cimoli & Marcer, 2014; Micheletti, et al., 2015). The DEMs are obtained by georeferencing the reconstructed 3D models through a set of Ground Control Points (GCPs) which are artificial or natural noticeable features present in the topography that are recognizable in the images. Since the 3D models generated with SfM are set on a local reference system, the georeferenciation process assigns real world coordinates to these GCPs and thus addressing all the model to real world coordinates consequently generating a DEM. Overall the SfM workflow applied to earth surfaces reconstruction can be seen in Figure 3.

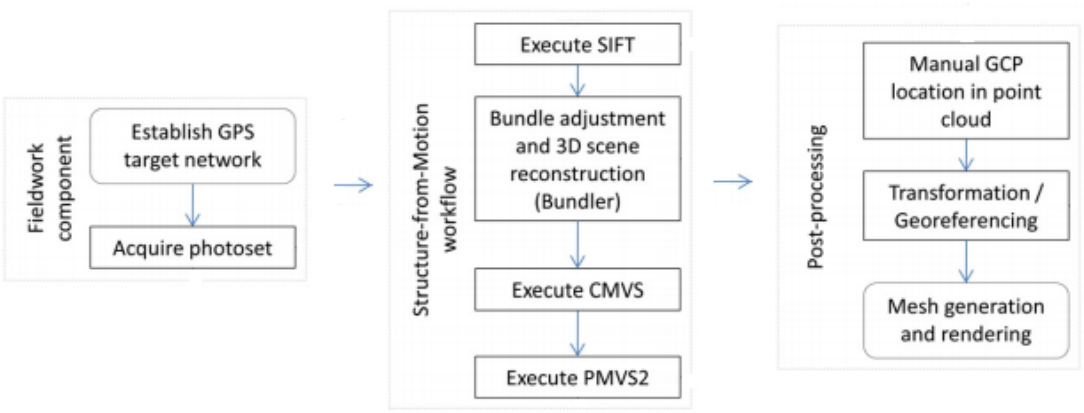

Figure 3: SfM workflow applied in a geosciences context (Westoby, et al., 2012).

Various SfM software are available including open source solutions like the Bundler technique or MicMac. Among the commercial programs we have Photoscan Pro by Agisoft or Pix4D. The present thesis uses Agisoft Photoscan Pro which is one of the most used by professionals in geosciences research concurring with the literature investigated and has been proved to be the best performer (Turner, et al., 2014).

The internal algorithmic details used by the Photoscan software package are considered proprietary and are not published by Agisoft, however the software claims improved and optimized algorithms from the

general common published standards aiming at favoring higher reconstruction accuracies over faster approaches in terms of calculation times.

2.4 Unmanned Aerial Vehicles (UAVs) Mapping Applied to Geosciences

Unmanned Aerial Vehicles (UAVs), or the commonly called drones, are relatively small flying vehicles that are remote controlled via manual or automated mode. Recently, these platforms have been extensively used to serve remote sensing and photogrammetry purposes. This is because compared to other methods they can provide large and accurate datasets, several possibilities of customizable settings using consumer grade equipment, relatively ease of deployment and low running costs. An extensive review on the state-of-the-art uses has already been done (Colomina & Molina, 2014).

In the field of environmental monitoring they have already been used for mapping purposes by applying digital photogrammetry methods like SfM (Hackney & Clayton, 2015). They present the advantage of being able to access and photograph areas that are inaccessible due to hazardous environments, of being remotely controlled for flying over large distances and to capture almost perfectly orthogonal imagery of land surfaces which noticeable improves the SfM performance using Agisoft for DEM reconstruction (Agisoft, 2013). Several studies have been done in this field by using UAVs combined with SfM methodology providing centimeter resolution DEMs of various kinds of surfaces (Ryan, et al., 2015; 2015; Dowling & Gallant, 2013; Mancini, et al., 2013; Harwin & Lucieer, 2012).

In the context mentioned above, an UAV survey is carried on by flying over the interested area acquiring a set of overlapping pictures taken from a camera. UAV mission planning is a critical phase for a successful DEM generation. Is optimal to have a degree of forward overlap (along the flight line) of 60-70 % and side overlap of 25-40% between the images acquired through the flight route (Agisoft, 2013). (Figure 4). It has to be considered that the UAV is a moving platform thus each frame from the camera has to be acquired on an adequate time interval to guarantee the image overlap.

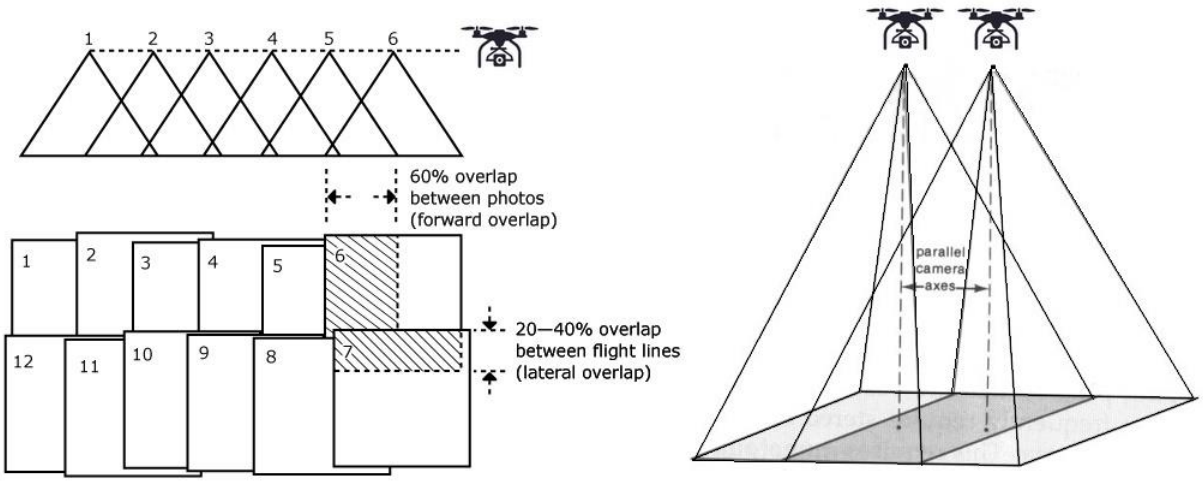

Figure 4: Optimal overlap conditions for aerial photogrammetry surveys.

The image footprint represents the ground level area covered by the image and is an important factor to consider in order to estimate the entire area intended to cover through the planned flight path and regulate it based on the personal mapping needs (Figure 5).

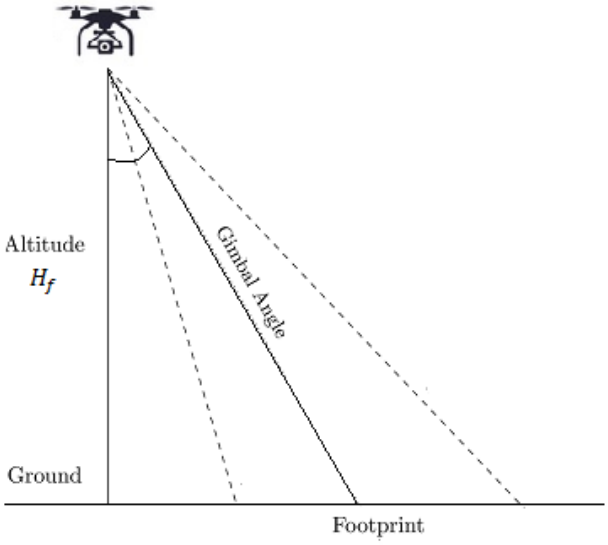

Figure 5: Illustration of the photographic footprint in an UAV aerial surveys.

The height and width of the photographic footprint can be calculated from the camera Field of View (FOV) and orientation as seen in Figure 5 by using the set of Eq. 4.

$$FOV_{width\,(height)} = 2 \times tan^{-1}\left(\frac{x_s\,(y_s)}{2 \times f}\right)$$

$$Footprint\ Width = H_f \times [\tan(\alpha + 0.5 \times FOV_{width}) - \tan(\alpha - 0.5 \times FOV_{width})] \quad (4)$$

$$Footprint\ Height = H_f \times \left[\tan\left(\beta + 0.5 \times FOV_{height}\right) - \tan(\beta - 0.5 \times FOV_{height})\right]$$

$$Photographic\ Footprint\ from\ an\ UAV = Height\ \times Width$$

Where x_s is the width of the camera sensor [mm], y_s the height of the camera sensor [mm], f the camera focal length [mm], H_f the UAV flying altitude [m] and α and β are the gimbal angles from the x and y axis respectively [*degrees*].

The resolution and accuracy of a DEM generated through SfM methodology heavily relies on the ability of the image to detect the smallest feature possible, in other words on the spatial resolution of the imaging system used. If a centimeter precision DEM is desired, the spatial resolution should be of the same order. A good way to measure the spatial resolution is the Ground Sampling Distance (GSD) which is the distance between pixel centers measured on the ground; the smaller the GSD, the better the spatial resolution achieved which leads to an increased amount of visible details. Given a defined camera setting for image

acquisition the GSD is directly related to the UAV flight height and it can be calculated from Eq. 5 (Lisein, et al., 2013).

$$GSD = \frac{Pix_{Size} \times H_f}{f} \quad (5)$$

Where GSD is the ground sample distance [cm/pixel], Pix_{Size} is pixel size [um/pixel], H_f the flying altitude [m] and f the camera focal length [mm].

It can be seen the relation between all the elements that have to be considered for a photogrammetric survey; the ground area to be covered by the mapping, the GSD (resolution of the mapping), the platform flying speed, the time interval between each frame acquisition, the camera internal and external parameters and the flying altitude has to be calculated based on each scenario.

These photogrammetric elements of the survey have to meet the technical capabilities of the UAV itself. For example in the case of multi-rotors UAVs (used in this thesis), the maximum flying time is heavily dependent on the payload the vehicle is carrying, on the type of batteries used and the multi-rotor specifications. Going into detail of the technicalities of flying UAVs goes of the scope of testing a photogrammetric method, still it can be concluded that mission planning is critical for these kinds of surveys both on a photogrammetric and technical level.

2.5 Advances in Image Pre-Processing to Enhance Automated 3D Reconstructions

The quality of the image and its characteristics are extremely important in the feature tracking algorithms used in the SfM methodology. Motion blur, sensor noise, erroneous depth of field or textureless images are some of the problems that these algorithms struggles to overcome. Due to the recent extensive use of these algorithms increasing importance is being given on the possible procedures that can be applied for enhancing SfM reconstruction performance by pre-processing and correcting the input images (Ballabeni, et al., 2015).

Some studies have been carried on regarding the use of polarizing filters or High Dynamic Range (HDR) photography for optimizing photogrammetry reconstruction performances mostly on cultural heritage objects and terrains (Guidi, et al., 2014; Kontogianni, et al., 2015). Testing these techniques in the current thesis work would not have resulted feasible for the following reasons. Polarizing filters significantly increases the amount of light needed in the photograph since some light is discarded in the polarizing effect. Thus, it would have required to at least double the exposure times in the UAV survey consequently risking blurred or overexposed images due to the UAVs movement and extremely reflective nature of snow. Polarization effect is also dependent on the angle of the incoming light in regards to the camera line of sight. On the other hand, HDR photography requires multiple frames of the same scene taken at different exposures to provide higher image dynamic range than the one allowed by the sensor. This process cannot be applied for a continuously moving platform like an UAV. Further recent studies shows that systematic errors in topographic models derived from SfM-UAV surveys might arise in the photogrammetric reconstruction due to the lens radial distortion (James & Robson, 2014).

However, SfM base algorithm is mostly used as a “black box” tool for geoscientists and surveying engineers in a DEM generation context. Some of these image pre-processing studies usually requires advanced skills

together with time consuming operations and are aimed at different specific kinds of surfaces and scenes. It is foreseen that the presented method could benefit from an image pre-processing workflow addressed at reconstructing snow surfaces acquired from UAV imagery in order to boost the SfM reconstruction performance but keeping the method swiftly applicable.

Chapter Key Points

- *HS* is extremely variable over space and time and is directly related to the SWE which is the most important snowpack propriety from a hydrological point of view. In order to calculate the SWE, ρ_s is also required. However, the spatial variability of ρ_s is much lower and several models are available that determine ρ_s from *HS* data. Therefore, the crucial matter is to be able to accurately estimate *HS.*
- *SfM* digital photogrammetry combined with UAVs can provide a powerful, cheap and more accessible tool for surveying in a remote sensing and geosciences context.
- *SfM* has well-known problems to reconstruct textureless surfaces like snow; issue that is accentuated under low luminance conditions. Its reconstruction with SfM is unprecedented.
- Increasing importance has been given to Image pre-processing since can positively affect SfM performances. It is foreseen that the current proposed method could benefit from a snow image pre-processing workflow to enhance snow surfaces reconstruction.

3 STUDY AREAS AND SURVEYING CONDITIONS

In order to put into practice and test the feasibility of the method, two fieldwork campaigns where carried on in two different Arctic regions. This consisted on a total of four fieldwork campaigns. In each campaign some snow covered areas of different sizes and kinds of snow surface where mapped during winter conditions in April 2015. The same process was repeated in summer during July 2015 for the same areas when the snow had completely or almost completely melted. From now on campaigns carried on during on during April 2015 are referred as winter campaigns (W) and in July 2015 as summer campaigns (S).

Some winter weather conditions like cloud cover and wind speed are considered limiting factors for the UAV and photogrammetry survey and therefore those are pointed out as surveying conditions. Cloud cover conditions defines the amount of light reaching the snow surface and consequently its luminance; luminance enhances the ability to discriminate fine detail by augmenting the contrast in the photographs (Jacobson, et al., 2000). This is particularly important for snow surfaces which have already a deficit in details. Nonetheless, wind conditions affect the UAV flaying capabilities and stability. Cloud cover is provided in a qualitative way which even tough is not very specific it can be forecasted all over the world and is very simple. The data was obtained from the nearest available weather stations in each region and from weather notes taken during fieldwork.

3.1 SVALBARD

Two small snow covered areas where selected in Breinosa, approximately 12 km from Longyearbyen, Svalbard (Figure 6) with an average elevation of 480 m a.s.l. The snow melting of these areas drains to Adventdalen valley.

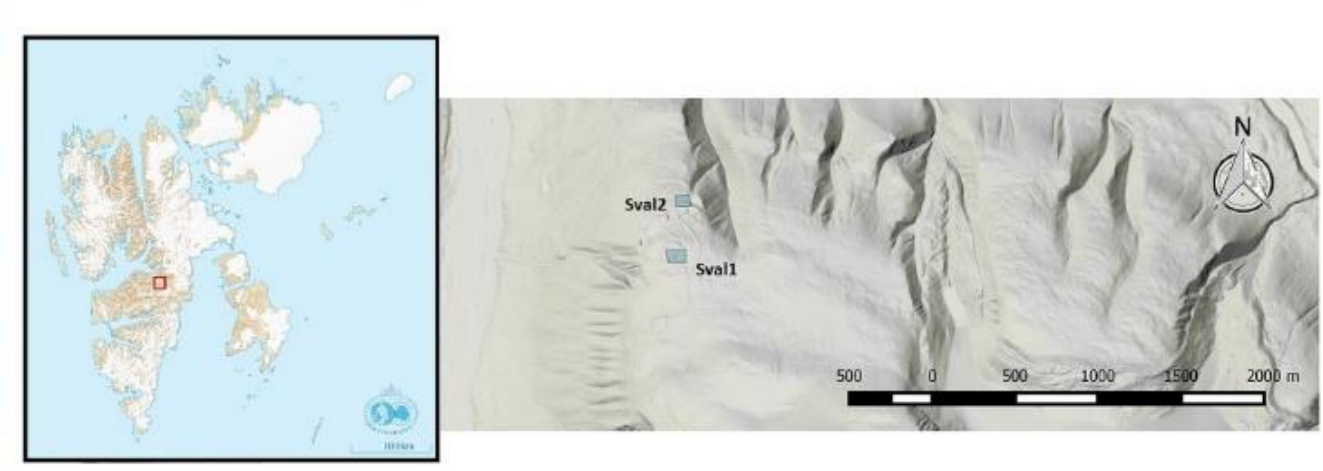

Figure 6: Location of Sval1 and Sval2 study areas in Breinosa, Central Svalbard.

The method could result useful for this region since most of the fresh water supply of Longyearbyen comes from snow melting and the catchment area is situated around 7 km from the test site. It is also particularly interesting to test the method in this region because of the high occurrence of avalanches which makes snow depth measurements unfeasible by normal means (Eckerstorfer, 2013).

Snow research is highly relevant in this region, and several studies regarding its snow characterization are available (e.g. Winther, et al., 2003; Eckerstorfer & Christiansen, 2011).The two study areas mapped are named and summarized in Table 1 in order to be able to reference them during the course of the thesis report.

Table 1: *Svalbard study areas summary table. The survey date is provided both for the Winter (W) and the Summer (S).*

Area Name	Approx. Center Coordinates (Lat/Lon)	Delimited Snow Area (m^2)	UAV Survey Date (dd/mm/yyyy)		Winter Weather Conditions
			W	S	
Sval1	78° 09′ 23″ N 16° 01′ 57″ W	6,700	5/4/2015	6/7/2015	Overcast/Fair 4.1 m/s
Sval2	78° 09′ 34″ N 16° 02′ 04″ W	900	9/4/2015	8/7/2015	Overcast 1.6 m/s

No noticeable intense snowfall preceded in the days before the winter mapping missions, therefore it has to be mentioned that the snow surface was generally very packed and sculpted by strong winds which entailed several sharp irregular ridges and grooves by the name of *sastrugi.* This phenomena is very characteristic on this region were winds are very strong and the climate is dry (Eckerstorfer & Christiansen, 2011).

A small snowfall and moderate winds preceded mapping of Sval2 providing a snow-dusted surface on top of the wind packed snow. Sval1 area is particularly interesting since the entire mapping was performed under very diverse luminance conditions which provided an interesting study case. Sval2 is a very small area but was characterized by being very steep with mostly bare soil underneath the snowpack. Sval1 is relatively flat but defined by the presence of small bumps reliefs in the terrain that generated a complex and irregular surface.

3.2 GREENLAND

In Greenland four areas where mapped approximately 30 km North-East of Sisimiut, West Greenland (Figure 7). One area was located at the end of Andenfjorden (2nd fjord) and the other three on the right orographic side of a valley that drains towards the Tasersuaq Lake.

It was considered interesting to investigate the method in this area since the Sisimiut hydropower plant is located nearby and harnesses the outflow of the Tasersuaq Lake for its energy production. Thus the method could be considered as resourceful tool for future applications and testing in case of a positive outcome. Little literature can be found on snow classification for the area, however snowmelt and hydrological studies have been performed in the vicinities (Bøggild, et al., 1999). The four sections mapped are enlisted in Table 2. In contrast with the Svalbard campaign, an intense snowfall of 15 mm in water equivalent over two consecutive days together with the presence of low speed winds of around 2 to 3 m/s resulted in a much more featureless, “soft” and smooth snow surface.

For area Green4 some stronger wind speeds preceded the mapping mission which marked some very small and lighter *sastrugi* features also called *ripples*.

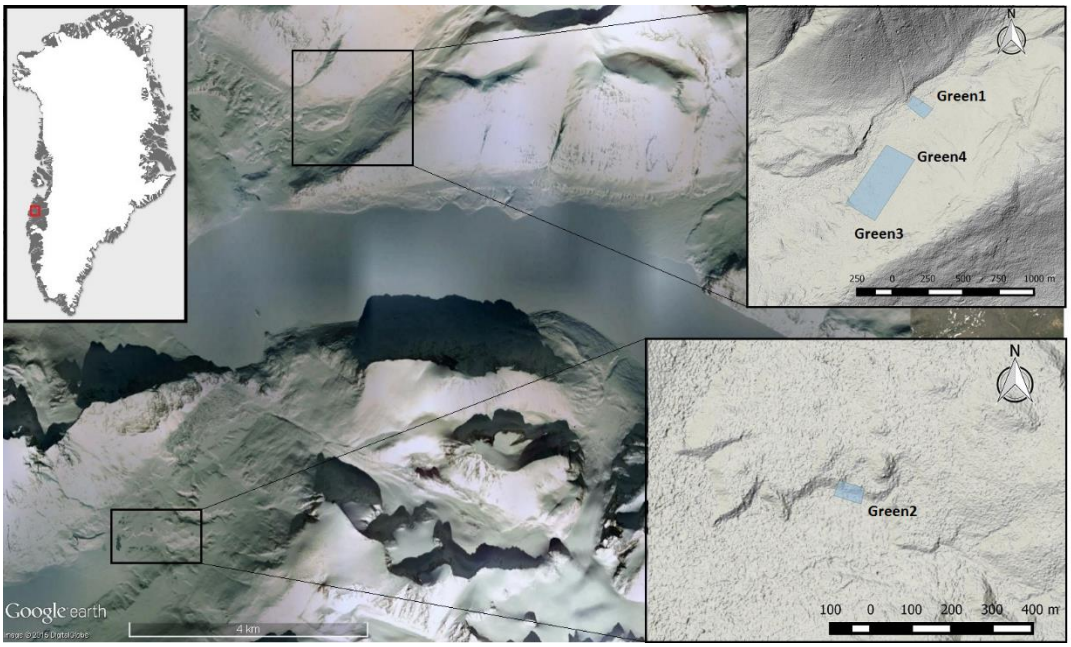

Figure 7: Location of the four Greenland study areas around the Tasersuaq Lake

Green1 is a moderately steep relief and during summer it was characterized by a vegetation covered topography. Since vegetation reconstruction is a well-known problem for SfM (Westoby, et al., 2012). The rest of the areas did not present any thick vegetation, the areas were covered by ground-level flora only.

Table 2: Summary table for the Greenland study areas. The survey date is provided both for the Winter (W) and the Summer (S)

Area Name	Approx. Center Coordinates (Lat/Lon)	Delimited Snow Area (m^2)	UAV Survey Date (dd/mm/yyyy)		Winter Weather Conditions
			W	S	
Green1	67° 10′ 53″ N 53° 14′ 07″ W	3,000	24/4/2015	28/7/2015	Fair 1.6 m/s
Green2	67° 06′ 56″ N 53° 19′ 19″ W	2,500	25/4/2015	27/7/2015	Clear Sky 3.7 m/s
Green3	67° 10′ 35″ N 53° 14′ 34″ W	51,000	25/4/2015	28/7/2015	Clear Sky 1.6 m/s
Green4	67° 10′ 40″ N 53° 14′ 22″ W	31,800	26/4/2015	28/7/2015	Fair/Clear Sky 5.8 m/s

Green2 is a soil terrain ridge that faces a glacier torrent lying on rock debris. Green3 and Green4 are two relatively big areas next to each other on the side of a glacier valley with a highly heterogenic topography made of soil, boulders and ground-level flora.

Chapter Key Points

- A total of 6 areas are subject of study with the purposes of testing the method over a wide range of different conditions. 2 near Longyearbyen, Central Svalbard and 4 close to Andenfjorden, West Greenland.
- The areas differ in terms of snow surface characteristics, complexity of the underlying topography and cloud cover conditions at the moment of the survey. The cloud cover is relevant since defines the luminance conditions of the survey.
- Testing the method over the Svalbard areas is considered particularly relevant since they are located just 7 km away from the Longyearbyen water supply. In Greenland the areas drains to the Tasersuaq Lake which is part of the hydropower system that supplies energy for the town of Sisimiut.

4 FIELDWORK METHODOLOGY AND EQUIPMENT

As previously mentioned a total of six snow covered areas and their corresponding underlying topographies where mapped. Different kinds of UAV platforms, cameras and mapping approaches were taken specifically for each case based on several planning factors and equipment availability. Some missions had to be completely re-planned with different equipment because of the technical difficulties encountered performing scientific fieldwork in harsh environments like the Arctic. The fact that some of the summer surveys are carried on by means of land-based SfM is not considered relevant since terrain DEM is "constant" and the objective is to be able to repeatedly determine snow depth by mapping the snow surface.

This chapter goes through the fieldwork methodology that was applied and the equipment used for testing the method over the six different areas. Each of the six UAV mapping missions was carried on in three stages: Allocation of GCPs, UAV survey and GPS survey. For each area also snow height (*HS*) and density (ρ_s) are measured over selected strategic points for validation purposes and for being able to calculate the SWE from the eventually estimated snow volume.

4.1 ALLOCATION OF GCPS

In this first stage the perimeter of the area is visually selected and artificial markers are placed as identifiable GCPs in strategic points spread across it. These points have to be recognizable in the UAV imagery since they will be used for the georeferencing process further on. In the winter campaigns the GCPs where mostly artificial because of the lack of identifiable features on the snow and consisted of self-made wood stakes or PVC tubes marked with crosses for precisely identifying one specific point on the surface. During the summer campaigns natural features like particularly shaped rocks where used for this purpose, they were marked with small dots using washable red spray paint. There is no specific rule for placing GCPs as long as the area coverage is wide, however was considered a good practice to place them in a gridded way for a more easy identification in the data processing phase. The total amount of GCPs placed for each area can be seen in the fieldwork summary Table 3. During this phase it was paid attention to avoid as much as possible footprints caused by walking on the snow while placing the GCPs since it would attribute a non-natural feature to the snow cover that could bias the SfM reconstruction process. The allocation of GCPs for each area can be visualized in Appendix 1 placed over the areas in some generated orthophotos.

4.2 UAV SURVEY

Different UAV platforms and cameras where used for the aerial imagery acquisition. This was dependent on the size of the area and on the equipment availability. The UAV platforms that were used for testing the method were a Walkera X350 Pro quadcopter, a DJI Spreading Wings s900 hexacopter and a custom build octocopter that can be seen in Figure 8. All models are multi-rotors which where preferred over airplane UAVs due to their higher stability and ease of use considering the relatively small areas intended to map.

Figure 8: Pictures of the used multi-rotors UAVs. The Walkera X350 Pro (bottom-left), the DJI s900 Spreading Wings (top-center) and the custom build octocopter (bottom-right).

The cameras utilized were a Nikon D3200 DSLR with a NIKKOR 18-55 mm lens for the DJI S900 and the custom octocopter. For the Walkera X350 Pro a lightweight GoPro Hero 3 was used. Cameras where attached to the UAVs at nadir direction either using professional gimbals for camera stabilization or custom made attachments aimed at dampening the effect of the multi-rotor vibrations on the image acquisition. The GoPro Hero 3 has an integrated intervalometer for automated repeat imagery acquisition over time, meanwhile for the Nikon D3200 a Polaroid shutter release timer was used for this purpose. All the platforms set-ups had to take into account the UAV maximum payload that trades off with available flight time. The UAV platforms used for each area mapped are shown in the fieldwork summary Table 3.

These experiments aimed to map as much as possible of the selected snow covered areas and to achieve centimeter resolution considering the amount of batteries and flight time permitted with the available equipment.

Image acquisition is a critical step for the proposed method since SfM heavily relies on the quality of the image, especially when the subject lacks natural features for being reconstructed. Therefore, camera internal parameters had to be set according to the desired GSD and the actual luminance conditions. Snow is a highly reflective surface therefore special attention is given to avoid overexposure of the images on clear sky days. However, this snow propriety is taken as an advantage and allows camera shutter speed to be set very high, which is extremely important to prevent blurred images caused by the aerial vehicle movement and vibrations.

Lower apertures are preferred (as long as there is no risk of underexposing snow free areas of the image in overcast days) since not only they provide sharper images and reduce optical aberration but also they enlarge the field of depth which reduces the risk of images being out of focus due to changes in the UAV elevation.

In the current experiments, the Nikon D3200 focus of the lens is set to infinity and the focal length was generally set around 18-20 mm which provided the widest footprint possible at a given altitude with the available lens. All images were shot in RAW format which enables a wider range of processing possibilities because acquires minimally processed and non-compressed data directly from the camera sensor. The GoPro does not allow any customization of the settings and has a fixed lens and aperture, everything else is set automatically, however the values usually ranged from 1/800 s to 1/950 s for the shutter speed and from 100 to 195 for the ISO sensitivity setting. The intervalometer in all cases is set to acquire one picture every second (1 Hz).

Table 3: *Fieldwork summary table. Equipment used, camera settings and GCPs allocated for each area mapped are enlisted for both winter (W) and summer (S). Camera settings display the focal length, the aperture, the shutter speed and ISO setting respectively. *Automatic states that it was set according to the GoPro automatic shooting mode. *Variable states that was continuously changing depending of the picture acquisition position during the land-based SfM procedure.*

<table>
<tr><th rowspan="2">Area Name</th><th colspan="2">UAV Platform</th><th colspan="2">Camera</th><th colspan="2">Camera Settings</th><th colspan="2">GCPs Allocated</th></tr>
<tr><th>W</th><th>S</th><th>W</th><th>S</th><th>W</th><th>S</th><th>W</th><th>S</th></tr>
<tr><td colspan="9">Svalbard</td></tr>
<tr><td>Sval1</td><td rowspan="2">Walkera X350 Pro</td><td>Custom Octocopter</td><td rowspan="2">GoPro Hero 3</td><td rowspan="2">Nikon D3200 18-55 mm lens</td><td rowspan="2">2.77 mm f/2.8 Automatic*</td><td>18 mm f/4.5 1/3200 s 200</td><td>12</td><td>11</td></tr>
<tr><td>Sval2</td><td>Land-based SfM</td><td>18-34 mm Variable*</td><td>4</td><td>8</td></tr>
<tr><td colspan="9">Greenland</td></tr>
<tr><td>Green1</td><td>Walkera X350 Pro</td><td rowspan="4">Land-based SfM</td><td>GoPro Hero 3</td><td rowspan="3">Nikon D3200 55-300 mm lens</td><td>2.77 mm f/2.8 Automatic*</td><td>92-300 mm Variable*</td><td>6</td><td>4</td></tr>
<tr><td>Green2</td><td rowspan="3">DJI s900 Spreading Wings</td><td rowspan="3">Nikon D3200 18-55 mm lens</td><td>18 mm f/8.0 1/3200 s 100</td><td>110-300 mm Variable*</td><td>12</td><td>10</td></tr>
<tr><td>Green3</td><td rowspan="2">18 mm f/18 1/800 s 100</td><td rowspan="2">59-300 mm Variable*</td><td>12</td><td rowspan="2">9</td></tr>
<tr><td>Green4</td><td>11</td></tr>
</table>

After having set the camera parameters, the UAV platform was remotely controlled to fly over the selected area with a similar pattern as shown in Figure 4. The flight speed is maintained at a lower value than the optimal in order to guarantee an abundant overlap of 50-80 %. To achieve a centimeter GSD with the current equipment the approximate flight altitude for each case was calculated using Eq. 4 and Eq. 5 but the vehicle was maintained at lower altitudes due to practical flying difficulties. The camera settings and systems used for each mapped area are shown in the fieldwork summary Table 3. Usually multiple flights had to be performed in order to cover the whole considered area.

For the topography mapping during summer, Sval2 and all the Greenland areas are mapped by means of land-based SfM due to the lack of an available multi-rotor caused by technical issues. This was done taking a similar approach as in previous work (Cimoli & Marcer, 2014). For the Greenland areas the highest available point for picture acquisition was around 1 to 1.5 km away of the study area therefore a NIKKOR 55-300 mm lens was used to aim at the winter mapping GSD.

From a practical point of view, considering the working temperatures experienced in the Arctic of around -10 to -25°C it was critical to maintain the LiPo batteries (Lithium Polymer batteries) of the UAV constantly warm until prior to use, otherwise their performance results heavily affected reducing the flight time near to zero.

Figure 9: Greenland winter mapping campaign; trying to repair UAV technical issues.

Furthermore, the UAV LiPo batteries were also covered using a minimum of insulating clothes during flight time. Another important practical aspect is the fixing of the lens. The multi-rotor vibration and movement changed the lens setting (focus and focal length) which caused the datasets of some flights to be completely unusable. A simple wide tape attached around the lens provided a simple solution to the issue.

4.3 GNSS Survey and Snow Probing

In this stage the objective is to obtain precise positioning of the points on the snow surface (and the underlying topography for summer) that were marked with GCPs. These positions will be then used for

georeferencing the acquired surface imagery. For this purpose a static GNSS survey is performed. This approach differs from other dynamic surveys applied in previous work (Cimoli & Marcer, 2014), since the receiver and the antenna remains fixed during the period of the observation and is set to acquire one positioning measure every second. The occupation time of the receiver and antenna varies depending of the desired accuracy; with higher acquisition times the accuracy increases due to the greatest sample set aiding the post-processing corrections.

The antenna and receiver used are a JAVAD Legacy receiver and a JAVAD RegAnt antenna and can be seen acquiring data for a specific GCP point in Figure 10. The antenna is placed over the exact marked point and since snow does not provide a solid and flat surface on slopes, the distance from the antenna measuring point to the snow surface is measured four times around the antenna. Also for the summer campaigns the distances from the ground or rock surfaces to the antenna measuring point are accurately measured.

Depending on the time available and the amount of GCP in the area, satellite data and geometry changes for each point are acquired for a period that ranges from 30 to 90 minutes depending on the time availability. The aim was to at obtaining centimeter precision or even in the order of a few millimeters by resolving the positioning systematic errors with a differential GNSS approach. This was afterwards done using nearby continuously operating reference stations as baselines that in this case operated both in Svalbard and Greenland. It is noted that for Green2 and Green3 land-based topography mapping practical difficulties did not allow for a wide and spread network of GCPs. This was mostly due to the big scale of the areas and the limited amount of time available to perform the survey.

Figure 10: JAVAD RegAnt receiving GNSS satellite data showing the antenna measuring point axis and measured distance to the snow surface (left). Snow probing procedure over a GCP location in Sval1 area (right).

Finally HS is measured using a centimeter scale avalanche probe over all the GCPs for a further validation of the estimated snow depths (Figure 10). For each point 4 measures around the antenna and a central measure in the in the measuring point axis.

Chapter Key Points

- The fieldwork procedure performed for testing the method consisted on 3 steps; allocation of GCPs, UAV survey and GNSS survey. This procedure was applied on all the 6 areas both in the winter and summer season for respectively mapping the snow surface and its corresponding underlying topography.
- Some of the mapping surveys are characterized by different equipment used, diverse camera settings and a varying number of GCPs allocated. Everything is enlisted in the fieldwork summary Table 3. The decisions depended on the size of the area, the luminance conditions and the equipment availability.
- Camera intrinsic and extrinsic settings are critical for a good quality photoset. Good quality photosets are mandatory for accurate *SfM* reconstructions.
- During the winter campaigns snow probing over the GCPs positions is done for a further validation of the *HS* maps.

5 DATA PROCESSING METHODS

This chapter goes through all the processing steps that were applied in order to estimate the snow spatial distribution from the data obtained during the fieldwork previously described.

The procedure basically consists on generating two DEMs for each area, one of the snow surface and the other of its underlying topography using SfM and then subtract them. This would provide snow distribution maps and thus volume estimates of the mapped area.

Since UAV mapping on normal terrain is already an established technique, the focus is given on describing the processes for mapping the snow surfaces, also because a normal terrain has a much lower temporal variability and for relevant areas good quality DEMs of terrains are usually already available.

5.1 FIELDWORK DATA ANALYSIS

In this section a preliminary analysis of the acquired imagery data is made. All photosets are analyzed and a manual image selection is done. Slightly blurred images caused by fast movements of the multi-rotors that were induced by wind gusts or other harsh maneuvers were eliminated. Also images that resulted out of focus because of the UAV loss of altitude were deleted from the datasets.

With a known reference measure on the ground that is visible on a UAV picture, is possible to calculate the GSD of the picture by comparing it to the amount of pixels it corresponds; by knowing the GSD and the focal length used to acquire the picture is possible to estimate the flight height of the UAV from Eq. 5. Here, Agisoft Photoscan Pro is used to estimate the average GSD and flying altitude for each area. The procedure also provides the degree of overlap of the imagery and thus the exact area that was covered by each survey.

5.2 GNSS POST-PROCESSING

All the GNSS points acquired for each area are processed in order to attain high accuracy positioning and thus reduce the overall error in the future georeferencing phase of the snow and terrain surfaces. For this purpose differential GNSS post-processing is applied using Leica Geomatic Office (LGO) software.

In the current work the Svalbard Satellite Station (SvalSat) is used as baseline for the Svalbard areas, the station is located approximately 5 km from the studied areas. For Greenland the Sisimiut reference station is used as a baseline and is located approximately 33 km from the studied areas.

The agencies in charge of the reference stations (Kongsberg Satellite Services and DTU Space) provided the precise location of their reference stations and the 24h positioning data acquired for each of the surveyed days. The data for each of the surveyed days is uncompressed using *Hatanaka* compression and decompression program providing the RINEX files (data interchange format for raw satellite navigation system data).

The GCPs data downloaded from the receivers was also transformed to RINEX using *jps2rin* program. Having all the raw data in RINEX allows to perform the correction of the acquired points. The corrections are computed trough LGO for each of the fieldwork days that a GNSS survey was performed. This is done using its corresponding 24h uncompressed RINEX positioning data file of the nearby reference stations together with their highly precise location estimate. Satellites from both the GPS and the GLONASS satellite system

are used for the computing process. The post-processing workflow was mostly performed following the LGO manual (Leica Geosystems, u.d.).

After having obtained the precise measured coordinates of each GCP, the antenna height measured during the GNSS survey is averaged and subtracted from the computed vertical height of each GCP. This gives the point height on the snow surface instead of the one in the slightly elevated antenna. The coordinates for each area in both seasons are finally exported in WGS 84 / UTM zone 33N for Svalbard and WGS 84 / UTM zone 22N for Greenland.

5.3 SNOW IMAGES PRE-PROCESSING

In this work the commercially available Adobe Photoshop Lightroom was used for processing the images which has already been pointed out as a useful tool for this kind of photogrammetric purposes (Giuliano, 2014; Ballabeni, et al., 2015). However, several other options are available for performing the same operations.

Considering the approaches that were taken by the previous studies, it was paid attention at the effects that these techniques where having on the processed images and the motivations behind them. Several tests were performed on the RAW snow imagery acquired considering these advancements on the image pre-processing field. In this context, each test consisted on modifying relevant attributes of a set of exemplar snow images and aligning them using Photoscan to count the number of matched patterns (or tie points) between them and observing the quality of the 3D point cloud in respect to the original surface; the more matched points between image pairs and the less noise in the 3D point cloud, the more successful the approach was considered. This testing was applied to several sub-sets for different areas and cameras. After performing the tests on the various image subsets a general protocol was developed for the current snow imagery datasets which increased the number of correct correspondences in relatively textureless areas and produced slightly denser and less noisy 3D point clouds. The protocol consisted in three steps and was applied over all the imagery datasets after having swiped them from blurred and out of focus images. The three steps are briefly depicted in the following lines.

Image content enhancement It was noticed from previous studies that image contrast, defined as the difference in luminance that defines an image object (Jacobson, et al., 2000), plays a fundamental role in feature tracking algorithms. This is because these algorithms extract features from pixel “intensity” levels in an image area and compares them with adjacent ones. An image histogram is graphical representation of the tonal distribution in a digital image and plots the number of pixels per tonal value. For images where snow is the dominant element (around 95 % of the winter dataset), the histogram is usually thin and bell shaped because of the relatively narrow range of tonalities. The aim is to set the histogram as centered as possible with an initial proper exposure correction. This allows to apply a high local contrast enhancement in the mid-tones of the image which increases the details in the snow textures while conserving the “global” contrast, thus safeguarding large scale shadows and highlights details.

In other terms, this process increases the contrast without reducing the image dynamic range, defined as the range of light intensities from the darkest shadows to the brightest highlights. This results in a wider image histogram compared to the non-processed one.

Optical correction Camera lenses always account for some degree of defect in the images, these defects are commonly termed aberrations (Wolf, et al., 2014; Jacobson, et al., 2000). Entering in the detail of such

a discipline goes out the scope of this work. However, two aberrations where noticed to cause noise and unnatural deformations in the 3D point clouds; radial lens distortion and vignetting which results in images that looked "curved" and obscured at the edges. These can be easily corrected using commercially or freely available tools like Agisoft Lens, Adobe Photoshop or MATLAB to mention a few. In the present work Adobe Lightroom was used for this purpose. Specifications of the camera model and lens are provided to the software that automatically corrects these two aberrations using its own internal correction model.

Noise reduction and sharpening Errors in the acquired images not only arises from camera optical issues, but also from the camera sensor. Image noise is defined as "unwanted variations in the response of an imaging system" and various types of noise exists (ISO 15739, 2013). A good brief summary of these is presented in a recent study related to the topic (Ballabeni, et al., 2015). Sharpening is a digital photography process that augments the edge definition in the images. The aim of the noise reduction and sharpening is to extract as much usable detail in the image while avoiding any oversharpened artifacts. Here, Adobe Lightroom noise reduction and sharpening are used in order to improve the image quality in the mentioned context. Depending on the characteristics of the area photoset, size of the smallest details to enhance, image frequency and noise tolerance the images are processed using digital photography sharpening and denoising workflows (Schewe & Fraser, 2010). Since photographed snow usually pictures a smooth monotone surface with some occasional small edged features that were shaped by the wind and the underlying topography, the aim was to sharpen these edges while trying to avoid producing unwanted noise in the smooth snow areas.

After applying these three simple post processing steps the images are converted into JPEG and are ready to be used in Photoscan Pro. The RAW format acquisition allowed for a wide range of manipulation actions without degrading the image quality as it would result when compressing the image to JPEG directly in the camera at the acquisition moment. Images could have also been converted to TIFF format which was tested to perform better by giving 3-5% more of matched points because of the higher bit depth. However, this involves extremely long computing times when taking entire datasets and therefore it was not considered a worthy trade-off in this case.

Furthermore, in order to test if the proposed protocol had an impact on the final DEM generation outcome, area Sval2 was completely reconstructed with completely unprocessed images and with processed images in parallel. The reconstruction process will be described in the following chapter.

5.4 DEMs GENERATION

In the following chapter the whole SfM process workflow using Agisoft Photoscan Pro aimed at reconstructing snow surfaces with the acquired imagery is depicted.

5.4.1 Sparse point cloud generation

After having processed each imagery dataset, Agisoft Photoscan Pro SfM pipeline is followed for each surveyed area. The procedure starts with the photo alignment which determines the camera position and orientation for each image and constructs a 3D model sparse point cloud on a local coordinate system (Figure 10). This is where the feature matching algorithm of Photoscan Pro that scans through all the imagery is executed. Slow but high accuracy alignment was preferred over fast computing times, but these times were noticeable reduced by an image pair preselection option (*generic*) which pre-matched image

pairs by using low accuracy first. This worked particularly well with highly overlapping and "ordered" datasets like the ones provided through an UAV survey.

The sparse clouds were then edited aiming at reducing reconstruction uncertainty. This is an important process since the model optimization and dense cloud reconstruction that will be applied further on depends on the quality of the initial sparse cloud (Agisoft, 2013). For this purpose the point clouds were manually cleaned of evident erroneous and out of place points and were then severely filtered of points with noticeable reprojection error targeting at obtaining accurate final results.

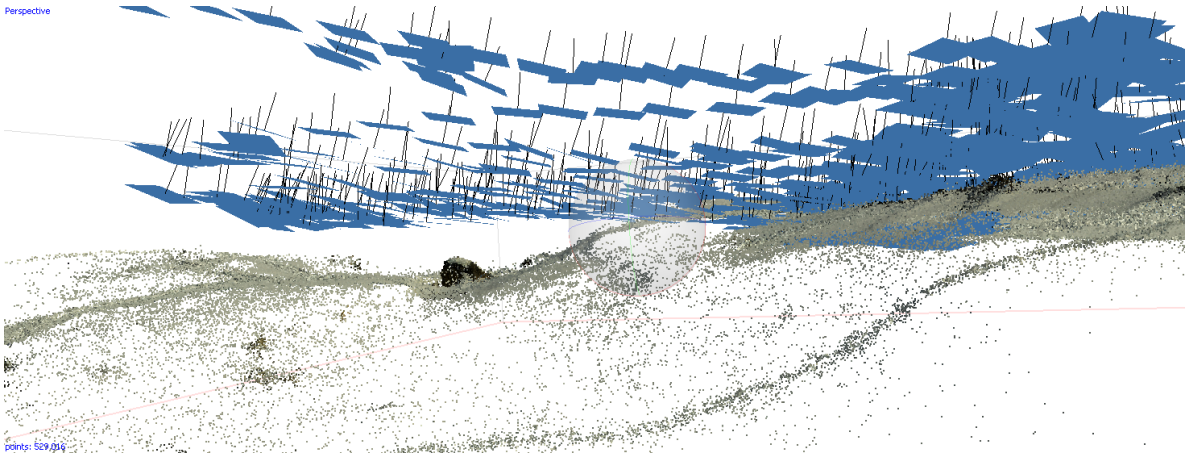

Figure 11: Example of a sparse point cloud and UAV camera positions on area Green1.

In cases where photosets where to big and computing times too long (~22 h for around 800 Nikon D3200 images), the pictures are divided in subsets (usually one set per UAV flight) and aligned separately. This provided a set "chunks" per area that are afterwards aligned by matching photos across all of them and then merged together to form the complete sparse cloud model of the area. This reduced overall computing times of around 60%. This was the case of Green 3 and Green4 that were divided in 3 chunks each.

5.4.2 Cloud georeferencing and model optimization

In order to georeference the 3D point clouds models generated for each area, the pixels corresponding to each GCPs mark are manually identified in the UAV imagery datasets. The corresponding high precision coordinates obtained from the GNSS post-processing are used to assign real world positioning to these identified known pixel points. With a minimum of 3 GCPs identified, all the points in the 3D model are then georeferenced through a Helmert-like 7 parameter similarity transformation in Photoscan Pro in the same CSR of the exported GNSS GCPs measurements.

This transformation only compensate for linear model misalignments between the generated surface and the known referenced GCPs. This means that the model can only translate, rotate and scale in order to minimize its misalignment with the known reference points. This process does not remove the non-linear errors that can arise during the photo alignment.

Using Photoscan Pro optimization the models are therefore adjusted of non-linear deformations by minimizing the sum of the reprojection error and the reference coordinate (GCPs) misalignment error (Agisoft, 2013). Basically this process performs a full photogrammetric adjustment that takes into account additional constraints introduced by ground control data (GCPs). Extrinsic and intrinsic parameters for all cameras estimates are optimized at this step, in contrast to the simple 7-parameter transform used in the default georeferencing.

The *optimization* also allows the GCP accuracy to be specified and thus this non-linear adjustment "weights" the degree of accuracy of the GNSS measurements for each GCP and applies its deformation taking it into account. The marker accuracy was therefore set according to the average quality of the GNSS measurements and by how well the markers could be identified in the images.

The two Svalbard areas Sval1 and Sval1 plus Green1 are georeferenced using some common GCPs that could be recognized both in the winter and the summer campaigns. This process is also known as *co-georeferenciation.* For area Sval1 three common points are used for georeferencing both the snow and the terrain surface. For area Sval2 the GCPs for referencing the snow surface are all in common with its corresponding topography. For area Green1 two GCPs are shared between the DEMs. The GCPs acquired in winter are thus used only for validation of the snow depth estimations.

Finally for each DEM the RMSE (see Eq. 3) of the northing, the easting and the altitude are computed using Agisoft Photoscan for each of the surveyed areas.

5.4.3 Dense cloud and mesh generation

The dense cloud reconstruction process is also relying on the quality of the sparse cloud and based on the estimated camera positions this process calculates the depth information for each camera to be combined into a single denser point cloud. All the areas were reconstructed at a *low* reconstruction quality because of the high computational power and the long processing times required in higher quality reconstructions (e.g. 30 hours for Green1). This process downscales the source images by a defined number of times on each side, usually is set four times for the GoPro Hero 3 (to 25%) and eight times for the Nikon D3200 (to 12.5 %) thus reducing the available GSD. However, considering the good quality of the imagery (especially for the Nikon D3200) and the low altitude in the range of 7 to 28 m this sub-pixel image resolution still resulted in a very detailed and accurate geometry.

Since the dense reconstruction algorithm calculates point depth maps for each photo, erroneous calculated points can be filtered using built-in Photoscan algorithms whose intensity is chosen depending on the photographed scene. Filtering is set to moderate since snow images usually present poor texture. This consequently sorted out outliers without eliminating small "real" details. Dense point clouds are further manually cleaned of evident erroneous points.

Triangular meshes of the areas where then reconstructed from the dense clouds with a high polygon count using a standard proposed Delaunay triangulation in Photoscan Pro.

5.4.4 DEMs and orthophotos production

DEMs of the snow surface and the underlying topography are finally exported in *geotiff* format from the generated georeferenced meshes of each area. The cellsize is set equal for both DEMs layers. The resampling factor of the cellsize is chosen based on the best outcome of the surface that resulted with lower resolution (either the snow or the terrain). They are exported in the same CSR as the determined

GCPs. Using Photoscan, low quality orthophotos are also produced for both the snow and terrain surfaces to provide quality control elements for a further validation of the snow depth maps (Appendix 1).

5.5 SNOW DEPTH DISTRIBUTION ESTIMATION AND VALIDATION

For each of the studied areas snow depth distribution is calculated using a MATLAB script shown in Appendix 3. Based Eq. 1, the script subtract the two aligned georeferenced grids. The same operation could be also performed more simply using commercially available GIS software (e.g. ArcGIS or GRASS GIS). In order to directly check the reliability and quality of the results, the HS estimates are compared with the set of snow depth probing measurements that where taken at the winter season GCPs positions. These points will be termed Quality Control Points (QCPs). Furthermore, the produced HS maps are overlapped to their corresponding underlying topography reliefs in QGIS and are compared side by side with the snow and terrain orthophotos shown in Appendix 1. This process assists in performing a qualitative assessment of the HS distribution maps and allows to identify common snow free features visible in both surfaces that can also be used as QCP.

When estimating the snow depth, the overall error derives from the two generated DEMs used for the subtraction. The error source on a SfM generated DEM is divided in two categories; the photogrammetric reconstruction error and the georeferencing error. The photogrammetric error essentially depends on the overall quality of the photosets, meanwhile the georeferencing error is alleged to be caused by the GNSS post-processing quality, the GCPs manual identification in the pictures and the antenna height point measurements. A clarifying scheme can be seen in Figure 12.

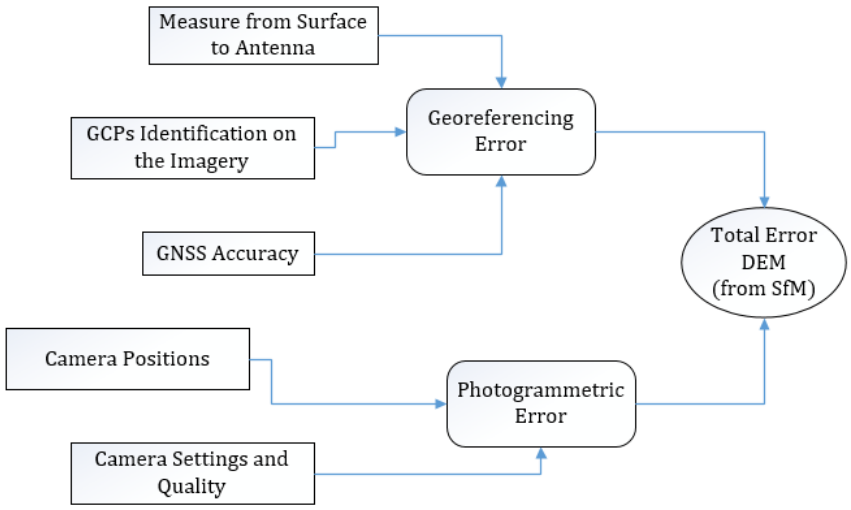

Figure 12: Schematization of the error components in DEMs generated through SfM.

The optimization process that was performed operated at both levels by correcting the photogrammetric error based on the georeferenciation accuracy. This procedure basically reduces the reconstruction error when the georeferenciation process has been done properly and markers could be precisely identified in pictures. As previously mentioned the optimization process is also dependent on the quality of the sparse cloud, therefore is also dependent on how methodologically well the images were acquired (constant focal length and proper camera positions) (Agisoft, 2013). Taking all this into account and considering that

Photoscan algorithmic details are not publicly available, it results very difficult to quantify the error attributed to each of the components. However, with the data obtained is possible to analyze and investigate the main source of error for each case.

Chapter Key Points

- Based on previous studies and on several tests, an image pre-processing protocol was developed which enhances image content, performs optical correction, denoises and sharpens snow imagery. This was applied to all photosets before the SfM processing.
- A test was performed on area Sval2 by generating the snow DEM with and without image pre-processing.
- In the georeferenciation process areas Sval1, Sval2 and Green1 were *co-georeferenciated.* This means that for each one of these areas the snow surface and its corresponding underlying topographies were georeferenced using common GCPs placed on features that were visible both in the winter and the summer campaign.
- All the georeferenced point clouds are optimized correcting non-linear deformations.
- Errors in SfM reconstruction arise from two components; the photogrammetric error and the georeferencing error. It results difficult to attribute values for each component, however is possible to speculate on the main error source.
- *HS* maps are generated by performing a DEM subtraction between the snow and topography surfaces. In order to validate the results, estimated *HS* and *HS* probed at some GCPs position are compared. These positions are termed Quality Control Points (QCPs). Furthermore the *HS* estimation is validated by qualitative comparison of HS with the underlying topography and snow free areas.

6 RESULTS AND DISCUSSION

In this chapter all the outcomes from each of the processing methods applied are shown and discussed while pointing out the main findings.

6.1 FIELDWORK DATA ANALYSIS

For each area the outcomes of the UAV survey is shown are Table 4. The exact mapped area resulted generally smaller than the delimited one, this was mostly due to technical flying capabilities. All areas mapped with UAV achieved a GSD in the order of the millimeter. The Greenland areas mapped via land-based SfM resulted in lower GSD due to the long distance from camera positions to the study area (1.5 km). Even though GCPs were marked in order to be able to visualize them on the images, some of them could not be properly identified. In the winter campaign this resulted mostly because of the UAV not properly passing by over the GCP or resulted to be out of the mapped area. For the summer campaign was mostly because some of the marked rocks could not be identified due to the small size of the marks considering the long distances of the picture acquisition. Table 4 shows the overall number of usable GCPs per area.

Overall the entire UAV imagery dataset comprehensive of all the areas was reduced of around the 7 % due to blurred or out of focus images (without counting completely unusable photosets of certain flights).

Topography of Green3 and Green4 share the same underlying topography since it was mapped as one unique surface during the land based survey.

Table 4: *Fieldwork data outcome summary table for both the Winter (W) and Summer (S) campaigns.*

Areas Name	Area covered (m^2)		GSD $(\mathrm{m}/pixel)$		Average flying altitude (m)		Usable images		Usable GCPs	
	W	S	W	S	W	S	W	S	W	S
Svalbard										
Sval1	6,200	8,987	0.003	0.003	6.23	22.4	912	194	9	9
Sval2	1,386	3,265	0.004	0.003	7.14	n/a	246	45	3	8
Greenland										
Green1	2,738	43,067	0.003	0.009	6.28	n/a	873	153	4	4
Green2	2,260	14,390	0.001	0.006	10.2	n/a	160	120	11	10
Green3	38,410	337,423	0.003	0.022	19.5	n/a	852	90	9	5
Green4	27,687		0.004		25.49		758		8	5

The image overlap outcome for each of the areas can be seen in Appendix 2. Some areas could not be completely mapped and present “holes” due to the lack of imagery in those spots. This is caused by the difficulty of manual flying and are issues that can be solved with automated and programmed flying modes. An example is shown in Figure 13.

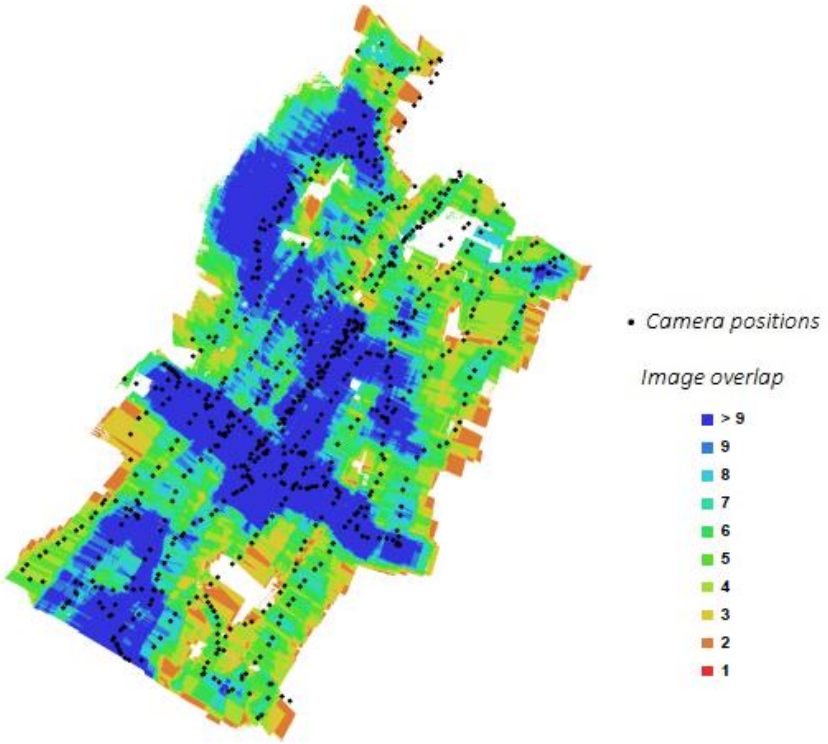

Figure 13: UAV flight route, camera positions and image overlap for area Green3. "Holes" corresponds to missing image overlap.

6.2 GNSS Post-Processing

Overall the GNSS positioning quality for all the areas is deemed to be of high accuracy. Table 5 shows the average position and height quality for each area. Centimeter to millimeter accuracy is reached. It can be noticed that accuracy is usually higher for the Greenland areas due to the higher acquisition times of more than 60 minutes that were applied during the GNSS Survey in the summer campaigns.

Table 5: GNSS post-processing positioning accuracy achieved for each area for both the Winter (W) and the Summer (S) campaigns.

Area Name	Average Position Quality (m)		Average Height Quality (m)		Average Position and Height quality (m)		Standard Deviation (Position + Height) (m)	
	S	W	S	W	S	W	S	W
Svalbard								
Sval1	0.008	0.003	0.018	0.005	0.019	0.006	0.014	0.006
Sval2	0.008	0.002	0.01	0.002	0.01	0.003	0.013	0.001
Greenland								
Green1	0.004	0.001	0.002	0.001	0.005	0.001	0.004	0.0005
Green2	0.003	0.002	0.002	0.001	0.004	0.002	0.002	0.001
Green3	0.004	0.002	0.002	0.001	0.005	0.002	0.003	0.001
Green4	0.005		0.001		0.005		0.006	

6.3 SNOW IMAGES PRE-PROCESSING

Depending on the image, the pre-processing procedure applied to the snow imagery increased the number of matched points between image pairs around 20 to 70 %. It also provided point clouds with less outliers (noise points seen around the correctly reconstructed surface) and better resembling the surface.

When applying the image content enhancement is important to aim at having a wide-and-centered histogram as can be allowed by the bit capacity of the image format. The fact that this process contributed to an increased amount of matched points is reasonable because having a wider histogram means that the image has more different pixel intensities and consequently provides more different and unique patterns for the feature matching algorithm. In order to properly pre-process images in batch mode it was important to group them under similar luminance conditions.

From the optical correction experiments it resulted particularly important to correct the lens radial distortion of the GoPro Hero 3 due to its extremely wide angle of 2.77 mm (see Appendix 4). This noticeably reduced the 3D point cloud deformations and noise. For the Nikon D3200 the results changed very slightly probably due to the narrow aperture used in most of the cases.

The noise that was more evident in the acquired UAV snow imagery was the *chrominance noise.* This appears as clusters of magenta and green colors in the image pixels and is caused by the inability of the sensor to differentiate colors in cases of low luminance (like the snow UAV imagery taken with small aperture and fast shutter speed). An evidence of this noise can be seen on Appendix 4.

Attention must be paid at avoiding the underexposure of small snow features and details provided by shadows or the overexposure of pure white extremely reflective snow zones.

The effect of this pre-processing approach can be seen applied to some example test in Appendix 4 for both the Nikon D3200 with the 18-55 mm lens and the GoPro Hero 3. It can be seen that in those examples the protocol resulted effective augmenting the amount of matched points. It can be noticed the different distribution of the points for the GoPro imagery with corrected distortion. Overall, it provided optimized results for pictures acquired with both high and low luminance at the moment of the UAV survey, especially for low luminance conditions.

Results from the parallel DEM processing of area Sval2 with and without image pre-processing provided a slightly better outcome for the cloud reconstructed with the pre-processing protocol. The non pre-processed reconstruction provided a point density of 232.226 $\mathrm{points/m^2}$ meanwhile the pre-processed reconstruction provided 306.07 $\mathrm{points/m^2}$. This resulted in a better available output resolution in Photoscan reducing the exported DEM cellsize from 0.066 m to 0.059 m. The generated surface can be seen in Appendix 4.

6.4 DEMS GENERATION

A total of 11 DEMs were generated from the four fieldwork campaigns. For each DEM, the RMSE of the northing, the easting and the altitude are shown together with the area total error and pixel error in Table 6. The total error represents the RMSE of the Euclidean distance from the reference GCPs to the corresponding estimated points in the 3D model. The pixel error represents the average reprojection error

for tie points present on each photo. Pixel error and point density are indicators of how well the surface was reconstructed from a photogrammetric perspective.

Table 6: Point density and accuracy for each of the generated DEMs.

Area Name	Point clouds density (points/m^2)		Easting error (m)		Northing error (m)		Height error (m)		Total error (m)		Pixel Error (pixels)	
	W	S	W	S	W	S	W	S	W	S	W	S
Svalbard												
Sval1	1412.3	273.6	0.055	0.007	0.08	0.034	0.06	0.036	0.122	0.05	3.8	3.1
Sval2	801.5	301.1	0.021	0.028	0.03	0.029	0.022	0.035	0.044	0.054	1.3	2.4
Greenland												
Green1	1518.5	163.77	0.042	0.11	0.03	0.11	0.01	0.16	0.05	0.23	1.1	4.3
Green2	1079.5	80.0	0.045	0.044	0.039	0.07	0.084	0.026	0.1	0.09	6.2	4.6
Green3	1095.0	126.66	0.029	0.05	0.034	0.15	0.02	0.02	0.05	0.16	3.3	2.0
Green4	653.297		0.040		0.021		0.024		0.052		8.1	

Overall, all the surfaces could be properly reconstructed and georeferenced. As expected, errors for areas mapped trough land-based SfM resulted higher than the UAV mapped areas. SfM was able to reconstruct snow surfaces for both high and low luminance days. No major drawback was noticed except for a slightly lower amount of matched points. This assessment still remains very qualitative but indicates that the applicability range in terms of luminance is not narrow.

Photoscan Pro non-linear photogrammetric correction reduced the error estimates in the range of 2 to 8 cm depending on the area. This optimization enhanced the results especially when the images were properly taken and the GCPs could be properly identified in the images. Furthermore, considering the good quality of UAV derived imagery and the good performance of the optimization photogrammetric correction, it can be inferred that the main error source resides in the georeferenciation component.

6.5 SNOW DEPTH DISTRIBUTION ESTIMATION AND VALIDATION

The estimated snow depth distribution for each of the studied areas is presented in the form of six HS maps overlapped to their corresponding underlying topographies from Figure 14 to Figure 20. In addition all the maps display the difference between the manually measured snow depths (HS_m) and the estimated snow depths (HS_{UAV}) at the probed GCPs positions. These points were termed QCPs and provide a discrete mapping of the error.

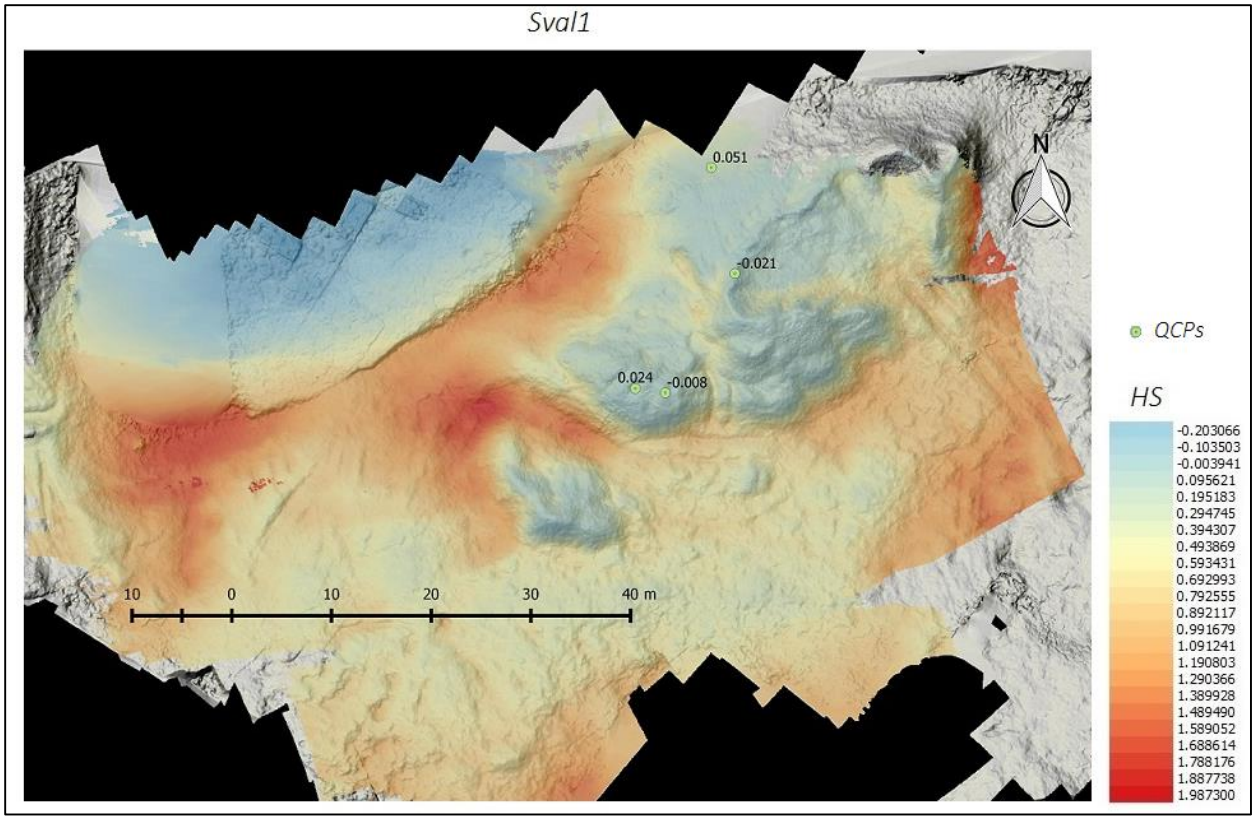

Figure 15: Snow depth (HS) map for area Sval1 overlapped to its underlying topography. The extremes in the color bar represent the maximum and the minimum values in the area.

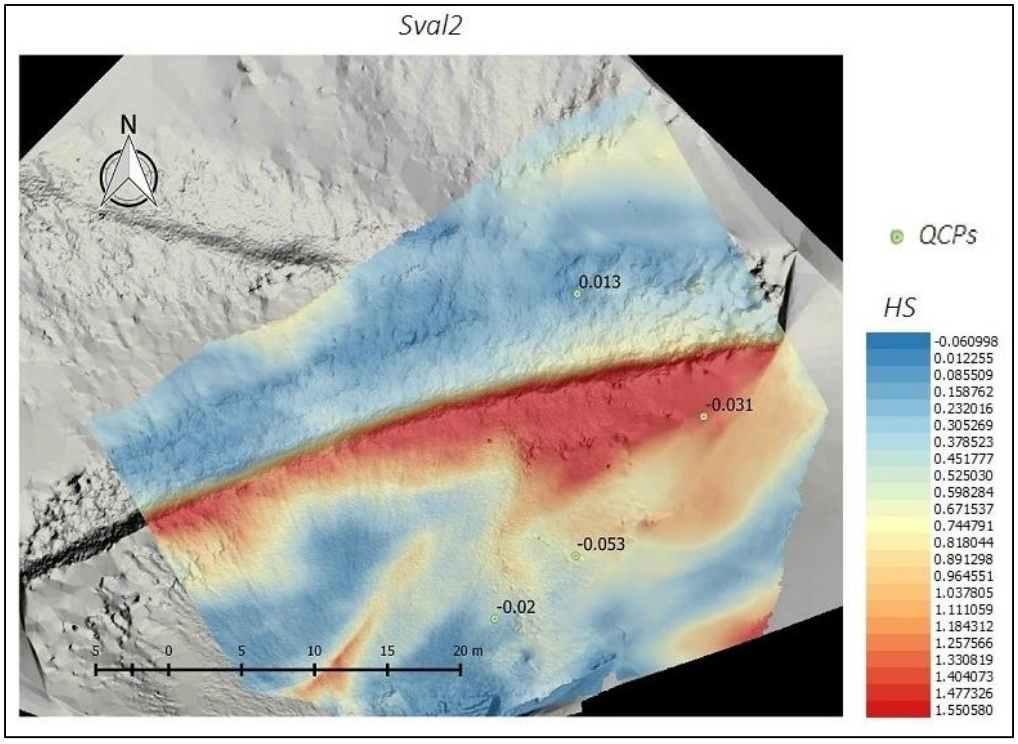

Figure 14: Snow depth (HS) map for area Sval2 overlapped to its underlying topography. The extremes in the color bar represent the maximum and the minimum values in the area.

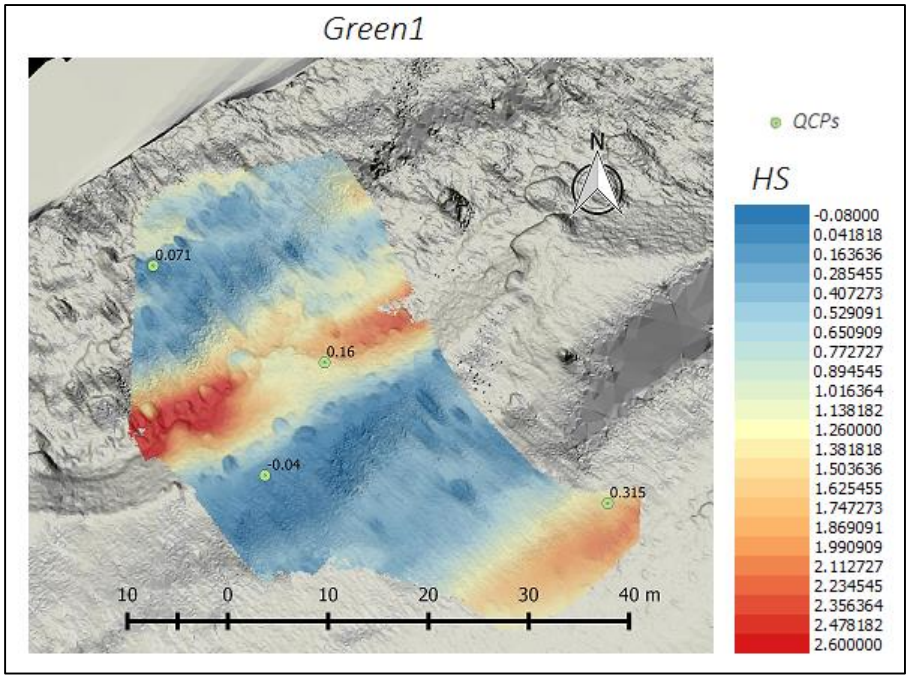

Figure 16: Snow depth (HS) map for area Green1 overlapped to its underlying topography. The extremes in the color bar represent the maximum and the minimum values in the area.

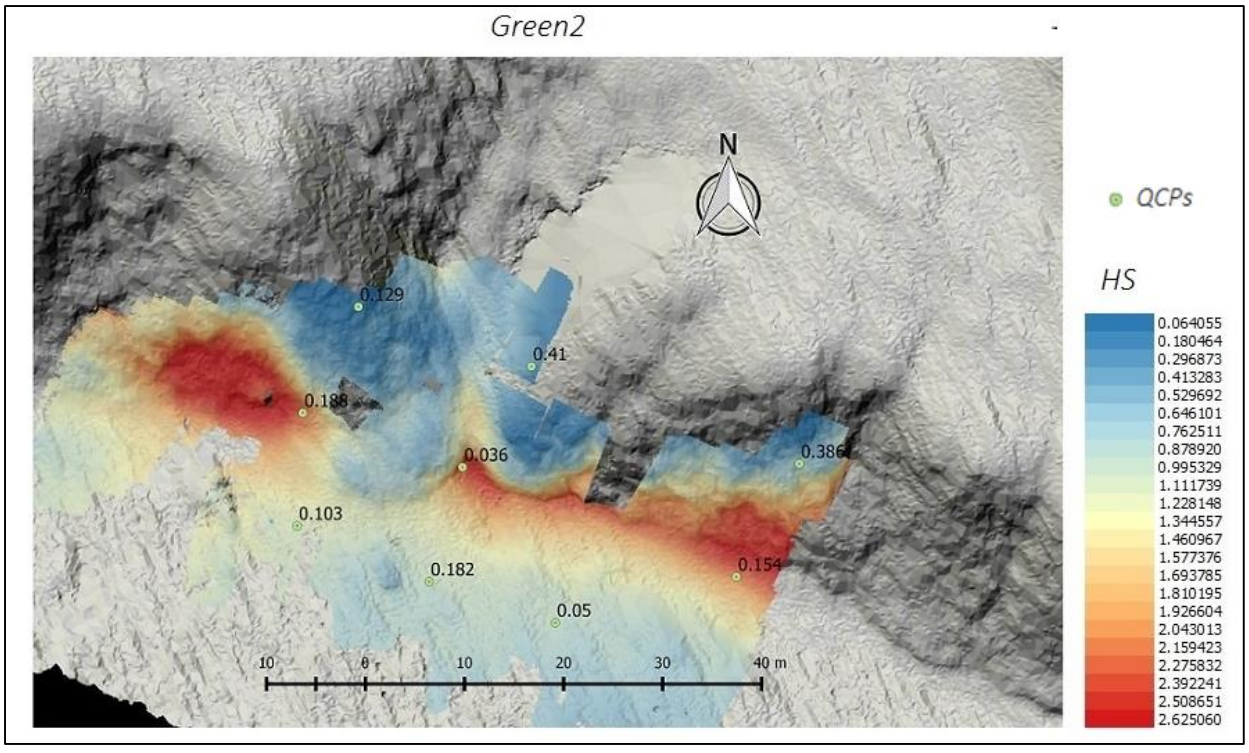

Figure 17: Snow depth (HS) map for area Green2 overlapped to its underlying topography. The extremes in the color bar represent the maximum and the minimum values in the area.

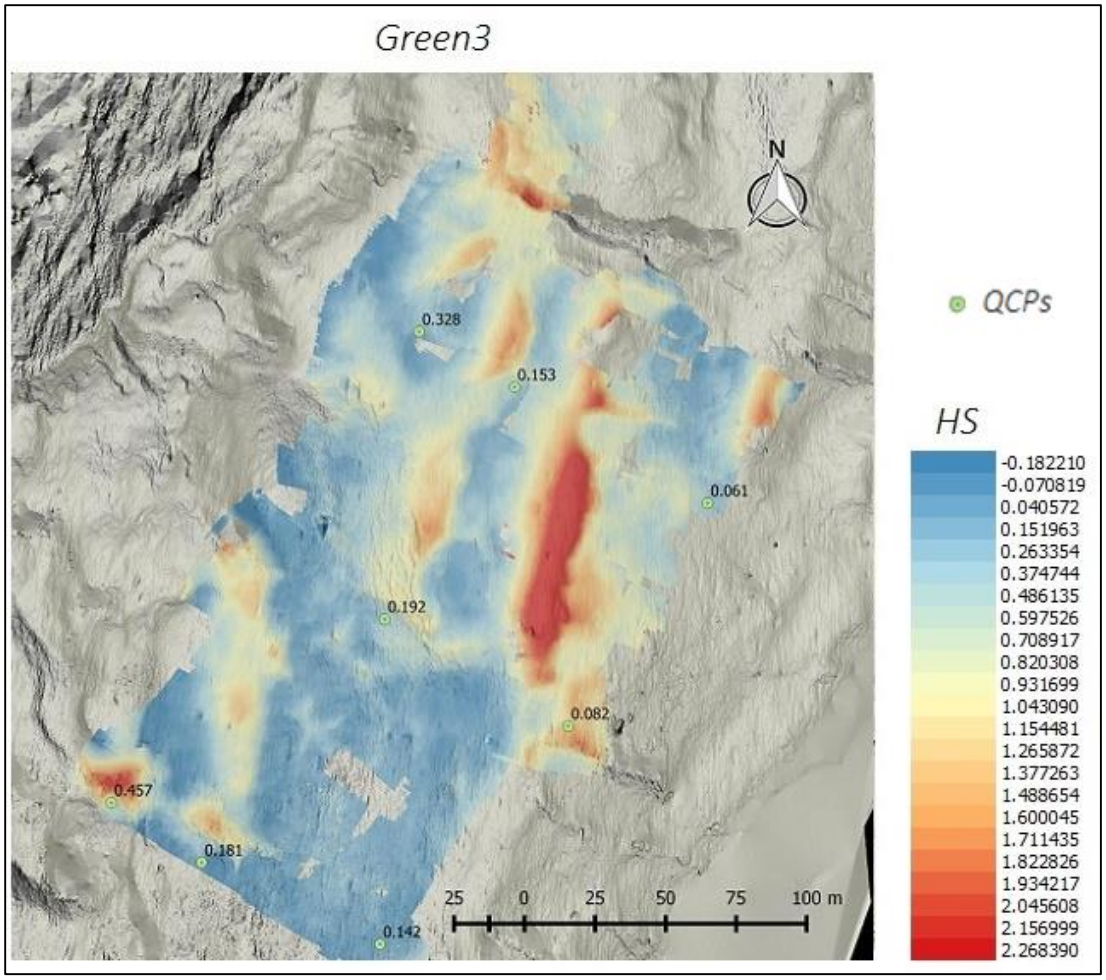

Figure 18: Snow depth (HS) map for area Green3 overlapped to its underlying topography. The extremes in the color bar represent the maximum and the minimum values in the area.

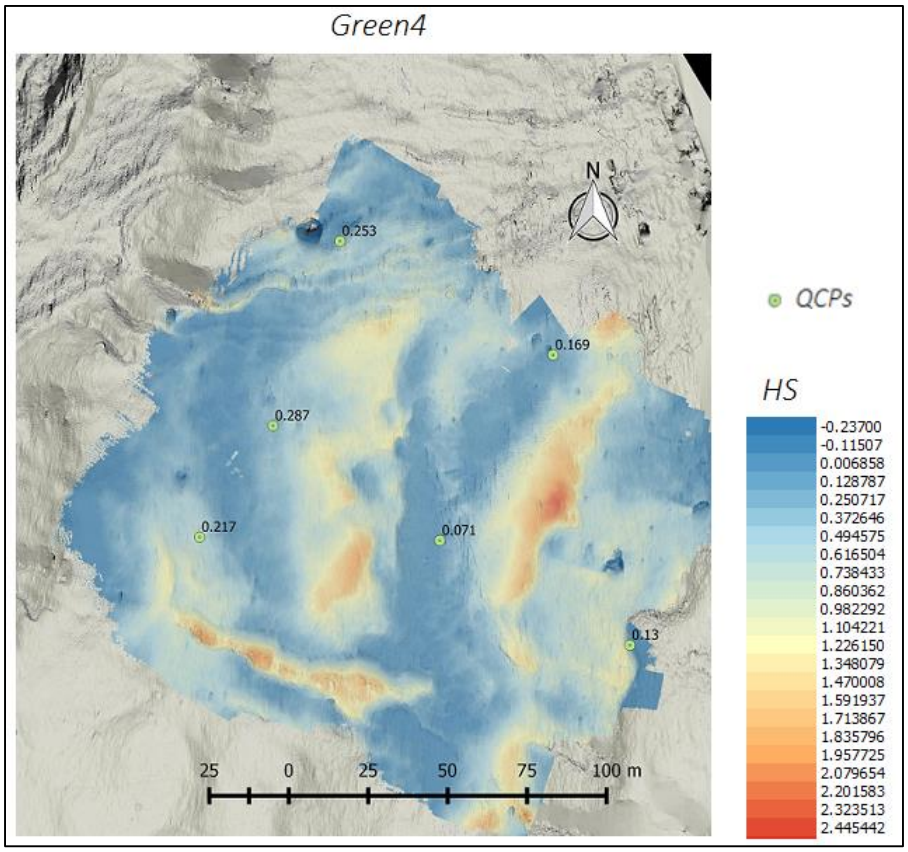

Figure 19: Snow depth (HS) map for area Green4 overlapped to its underlying topography. The extremes in the color bar represent the maximum and the minimum values in the area.

For each area the average of the difference between HS_m and HS_{UAV} along with its standard deviation is presented in Table 7. The table summarizes the outcome of the validation procedure.

Table 7: Outcome of the validation procedure trough QCPs for all areas.

Area Name	Number of Quality Control Points (QCP)	Average difference $HS_m - HS_{UAV}$ (m)	Standard deviation (m)
Svalbard			
Sval1	4	**0.011**	0.0280
Sval2	4	-0.026	0.0277
Greenland			
Green1	4	0.1265	0.1499
Green2	9	0.1829	0.1350
Green3	8	0.1995	0.1318
Green4	7	0.1878	0.0803

The mapping resolutions and surveying conditions for each area are enlisted in Table 8. This table summarizes the mapping outcome for all the areas under the different surveying conditions.

Table 8: Summary table comparing area covered, resolution achieved and snow surface type over all the surveyed areas.

Area Name	Area covered (m^2)	Resolution (m)	Winter luminance conditions	Snow Surface Type
Svalbard				
Sval1	6,200	0.06	Overcast/Fair	*Sastrugi*
Sval2	1,386	0.06	Overcast	*Sastrugi* and snow dusting
Greenland				
Green1	2,738	0.1	Fair	Fresh and smooth
Green2	2,260	0.1	Clear Sky	Smooth
Green3	38,410	0.09	Clear Sky	Smooth with light snow *ripples*
Green4	27,687	0.09	Fair/Clear Sky	*Sastrugi* and light snow *ripples*

Qualitatively the snow accumulation is well represented over the topographies for all the areas. High snow accumulation zones are correctly linked with topography depressions and with snow-drift filled terrain hollows. Correct details of snow accumulation over small depressions can be distinguished on the maps at a very small detail.

As previously mentioned, it results very difficult to assess the origin of the errors and to distinguish between the photogrammetric and the georeferencing error. However, is possible to speculate on the main error source for each of the studied areas.

As seen from Table 7 areas Sval1 and Sval2 responded extremely well at the QCPs validation. For area Sval1 the presence of a nearby lake provided an extra positive quality indicator by correctly showing that the snow depth remains constant over it meaning that the DEM does not have present any kind of inclination bias (see Figure 1).

Greenland areas still responded very well to the QCP validation (Table 7). However, the average difference increased of one order of magnitude. As can be seen from Table 6 the snow surfaces where accurately mapped with the UAVs providing accuracies of around 0.05 to 0.10 m with a well distributed network of GCPs (see Appendix 1). The same cannot be said for some of the corresponding summer mapped areas. In these cases the increase of the total error estimated is attributed not only to the poor quality of land-based SfM picture acquisition perspective compared to the aerial SfM, but also to the poor distribution of GCPs. This effect can be particularly seen on Green3 and Green4 areas. The poor GCPs coverage for such and

extensive underlying topography can be seen in Appendix 1. From Figure 18 and Figure 19 it can be observed that HS_{UAV} is underestimated in the north-west side of the mapped areas by providing high positive values in the QCPs. This suggests that the DEM has been slightly tilted towards south-east where there is a bigger concentration of GCPs. Therefore, the underlying topography DEM of Green3 and Green4 resulted biased.

In contrast with the previous mentioned areas, Green2 provided a well-distributed grid of GCPs over the snow sector that was mapped in winter (see Appendix 1). Some parts of this area are characterized by a vegetation covered topography. In this case it can be observed that Green2 errors are associated to HS_{UAV} underestimations caused by the presence of bushes and thick vegetation (see Appendix 1). Bushes and thick vegetation are reconstructed as a bulky continuous surface in SfM, thus the DEM reconstruction process does not allows to differentiate the ground level for those areas and provides a more elevated DEM. This observation is supported by the fact that also all the QCPs are positive indicating that the snow depth is underestimated.

For area Green1 seen in Figure 16 it could not be assessed the source of such a high validation error of 0.315 m in the south-east sector since the nearby snow free small boulders provided HS_{UAV} in the order of the millimeters. The option of an incorrect probe measurement or field book note annotation is not discarded.

Further comparisons with the snow and topography orthophotos for all the areas allowed the identification of various snow free features like boulders or elevated snow free areas that could be also used as Quality Control Points (QCP). Over these snow free features the snow depth was expected to be zero. The actual estimates of these values ranged from -0.03 to 0.07 for areas Sval1, Sval2, and Green1 and from -0.08 to 0.19 m for areas Green3 and Green4. Area Green2 did not provide any additional QCPs. These observations matched the order of magnitude of the average difference estimated through the probed QCPs.

Is observed that the co-georeferencing approach provides much better results by mitigating the georeferencing error component; this is an extremely relevant and interesting finding. This can be observed from the outcomes of the DEMs generation in Table 6. The total errors estimated trough the RMSE for the DEMs of Sval1, Green3 and Green4 are in the same order of magnitude. Still, the QCPs validation shows much better results for area Sval1.

The maximum output resolution in Photoscan Pro is dependent on the amount of matched points. Thus, is dependent on the SfM reconstruction performance. The SfM performance was expected to be limited by the luminance conditions and the snow texture type. However, high resolutions of 10 cm and below are achieved over all the mapped areas independently of the different luminance conditions and snow surfaces types. It can also be observed in Appendix 1 that for area Sval1 the orthophoto varies in tonalities, this is due to change in luminance conditions at the moment of the survey. Is believed that for the Greenland areas the resolution resulted slightly downgraded due to the land-based SfM carried on during the summer campaign. This is caused by limitations to access proper camera positions during the survey. The resolution of the surveys did not resulted affected by the low quality of the GoPro Hero 3 in comparison to the Nikon D3200 DSLR. The reason behind this lays on the UAV flying altitude. In a photogrammetry context, high quality cameras obviously perform better and would be able to fly much higher without compromising the resolution. However, it has been proved that the same results can be achieved by modifying the survey parameters in e.g. the flying altitude. Topographies and snow surface types also changed drastically on the

different surveyed areas without noticeable changes in the outcomes, however this has to be further investigated.

Chapter Key Points

- From the fieldwork data analysis it can be observed that the sizes of the mapped areas ranged from 1,386 to 38,410 m^2 and the GSD ranged from 0.001 to 0.004 $\mathrm{m}/pixel$ (Table 4).
- The GNSS post-processing on the measured GCPs achieved centimeter to millimeter accuracy depending on the time invested for each measurement (Table 5).
- The image pre-processing protocol increased the number of matched points between image pairs of around 20 to 70 % depending on the images. It was observed for one test area that the increase in matched points has an overall effect in the output DEMs resolutions. In the test with and without pre-processing for one area, the resolution slightly augmented from 0.066 m to 0.059 m in grid cellsize for the one with pre-processed imagery.
- A total of 11 DEMs were generated. 6 snow surfaces and 5 underlying topographies. The accuracy of such DEMs ranged from 0.04 m in the best case to 0.23 m for the worst case (Table 6). The lower accuracy is attributed to the land-based SfM surveys.
- The estimated snow depth maps responded well to the Quality Control Points (QCPs) validation. Depending on the area the average difference between probed and estimated HS varied from 0.01 m for the best case area to 0.19 m for the worst case area (Table 7) meanwhile the spatial resolution ranges from 0.06 to 0.1 m (Table 8). The worst cases are attributed to the poor GCP network of the underlying topography resulting in a biased DEM.
- Vegetation covered topography caused snow depth underestimation for one area.
- The areas were *co-georeferenciation* was applied responded much better to the validation control. This procedure drastically mitigates the georeferencing component of the error.
- The method established good results over a wide range of snow surface types, luminance conditions, underlying topographies and equipment used; this outlines the method application flexibility.

7 CONCLUSION

Snow cover plays a critical role in the climate, ecological and hydrological systems both on a regional and a global scale level. From a hydrological perspective, the SWE is the most important snow cover propriety. This volume is termed SWE and its estimation is extremely relevant for civil purposes (e.g. drinking water supply, hydropower generation and water resource management systems), but also in various hydrological and environmental research sectors. SWE is directly related to the snow depth distribution, thus estimating snow depth results of extreme interest. However, the snow depth is also highly variable over space and time and current traditional and state-of-the-art methods (e.g. point probing, LiDAR, GPR, remote sensing from satellites or manned airborne solutions) for monitoring snow in this context either lack in mapping resolution, in accuracy or either they come at very high costs. The current thesis objective was to design, test and report a new methodology for estimating snow depth spatial distribution that could render snow monitoring swiftly applicable, accurate and with low running costs. A methodology was designed and tested and involved the combinations of two thriving technologies which are SfM digital photogrammetry together with the use of UAVs. The concept behind the method was to subtract the DEMs generated through SfM and UAV imagery of the snow surface and the underlying terrain for estimating the snow distribution.

In order to validate the method, the procedure was tested for six different snow covered areas over two different Arctic regions. The snow surfaces of these areas and their corresponding underlying topographies were mapped and subtracted. The areas differed in terms of snow surface type, underlying topography complexity, surveying conditions and equipment used. Surface type ranged from highly sculpted and wind-packed snow surfaces, to fresh and smooth recently fallen snow. Surveying luminance conditions observed consisted both in bright clear sky days and overcast days. The camera equipment used were a cheap (in terms of UAV payload) GoPro Hero 3 and a high-end DSLR Nikon D3200. This provided a testing sample that could also allow to test the flexibility of the method.

The tests were performed over small scale areas that in the final outcome ranged from 1,386 to 38,410 $\mathbf{m^2}$**.** However, the final aim of the project is to provide an operational method that can be applied for large realistic case scenarios and commercial solutions.

The main findings of this first method application and the weaknesses that needs to be addressed for a future commercial applicability are inquired in the following five questions.

Is SfM digital photogrammetry able to reconstruct snow surfaces?

It was well-known that digital photogrammetry mapping applied to surfaces like snow was unprecedented without expensive manned airborne approaches and was considered problematic due to the textureless nature of this kind of surface. This thesis proved that not only is possible to reconstruct snow using SfM with a proper image acquisition and processing procedure, but is also feasible over a wide a range of snow surface types and luminance conditions. SfM requires patterns in the images to be recognized for reconstructing scenes. The patterns are created from textures in the images and from luminance that generates contrast between them. The reconstruction has been successful from *sastrug*i sculpted snow to freshly fallen and smooth snow. Also, the reconstruction performed well for both high luminance clear sky days and low luminance overcast days without major drawbacks on the worst case scenario.

Has the newly proposed method been successfully tested?

As previously mentioned, the method has been tested over a set of six different snow covered areas. Overall, all surfaces (both snow and underlying topographies) were successfully mapped with total accuracies ranging from 0.04 m in the best case to 0.23 m for the worst case. Best cases are usually the outcome of UAV SfM based survey, meanwhile worst cases comes from land-based SfM surveys. Land-based SfM surveys were performed exclusively when mapping some summer topographies due to UAV technical issues.

The final results were provided in the form of snow depth distribution maps. The maps were validated in three ways; by qualitatively observing snow accumulation zones, by comparing estimates on snow free areas and trough a set of precisely known Quality Control Points (QCPs) spread around the area with known probed snow depths.

The visual qualitative assessment indicated appropriate snow accumulation zones. The average between the measured snow depths (HS_m) and the estimated snow depths (HS_{UAV}) ranged from 0.01 m for the best case area to 0.19 m for the worst case area. For the worst cases it was observed that the error source derives from the land-based SfM summer campaigns that provided poor quality photosets and poor georeferenciation network coverage. For some cases this resulted in slightly biased topography DEMs that caused snow depth to be underestimated. In one case SfM was not able to properly reconstruct thick vegetation covering one area resulting as well in a snow depth underestimation over some QCPs. In terms of resolution, the maps cellsize ranged from 0.06 m for the best cases to 0.1 m for the worst cases.

Considering the accuracy and resolution achieved, this easy applicable method that required only consumer purchasable equipment can be compared with other very expensive state-of-the-art solutions (e.g. airborne LiDAR) (Deems & Painter, 2006). Therefore, this first attempt in realizing the method can be considered successful and the methodology shows tremendous potentialities for snow mapping.

It might be argued that the sample size for each area is low, but this is compensated by the fact several areas where mapped and still provided results in the same order of magnitude.

Furthermore, it has to be mentioned that in the performed tests worst case resolution can definitely be improved with a better topography mapping (e.g. with a proper UAV campaign).

Is the suggested image pre-processing protocol really useful?

In this thesis work a simple image pre-processing approach aiming at augmenting SfM reconstruction performances was suggested. The approach moderately improved matching points between random image pairs of around 20 to 70 % depending on the image. The procedure resulted to have better outcomes for images taken at overcast days and for images taken with a GoPro Hero 3. A further test performed showed that augmenting the number of matched points increases the point densities. It resulted that while this does not directly affect error estimations it affects the maximum output cellsize obtained with Photoscan Pro; therefore affects the mapped area spatial resolution. On a small test performed in area Green2 the output cellsize changed very slightly from 0.066 m to 0.059 m which is not a drastic improvement. Although, the impact of this is expected to be more influent when mapping larger scale areas.

From a hydrological point of view, the spatial resolution might affect the uncertainty of volume estimations; especially for complex underlying topographies where snow depth can significantly vary at micro-scale

level. However, the spatial resolution results even more important in a snow sampling context for various purposes as observed in some other studies (López-Moreno, et al., 2013; Liston & Sturm, 2002).

The use of GCPs involves too much time and effort. Can something be done?

In this first method approach the mapped areas were georeferenced through the use of GCPs. Each GCP observation period lasted around 30 to 60 minutes and involved constant movement of the device from one point to another. In order to keep the method swiftly applicable, this issue needs to be overcome.

In the present study it was observed that *co-georeferenced* areas provided much better snow depth estimates. This was the case for areas Sval1, Sval2 and Sval3. *Co-georeferenciation* consists on georeferencing both DEMs with common visible features of known precise location. In the present study it was observed that it noticeably mitigated the georeferencing error by rendering the DEMs subtraction relative. The answer to overcome this GCPs procedure lays in the co-georeferenciation since common visible points can be acquired only once and then can be repeatedly used for georeferencing the time variable snow surfaces. These points could be natural features, or artificial placed markers around the continuously surveyed area.

Furthermore, recent topography mapping studies using UAVs have been evaluating the possibility to add on-board Real Time Kinematic (RTK) GPS to the UAVs. This would provide the positioning of the camera at each taken frame that can be used in Photoscan to directly georeferenciate the camera stations instead of the images (Solbø & Storvold, 2013; Turner, et al., 2014). These approaches still does not provide the needed accuracy in terms of GNSS positioning, but is expected that these technological challenges will be surpassed in the future and GCPs will not be needed anymore.

Can the method be applied in a realistic scale scenario in harsh and difficult environments like the Arctic?

In the present thesis the method was tested over relatively small scale areas compared to catchment wide scale areas. Also, the method was tested under relatively low speed wind conditions compared to the often higher speed winds observed in Arctic environments. In order to render the method operative in such environments, these issues needs to be addressed.

Recent technological advances shows that increasing attention has been given to this kind of problematic by investigating powerful UAV solutions especially designed for Arctic and Antarctic research (Funaki, et al., 2008; Solbø & Storvold, 2013; Ryan, et al., 2015). For example, some of these proposed fixed wings UAV models are able to fly over straight distances of 500 km and have been tested to work under high speed winds of 22 $\mathrm{m/s}$.

It might be argued that the high spatial resolution achieved was the outcome of a low flying altitude which provided a high GSD, thus higher flying altitudes aimed at mapping large scale areas would not achieve the same quality results. This argument results invalid since in the current test the images were downscaled of around four to eight times during the dense cloud reconstruction process. This means that basically using the same settings used in this experiment (with the Nikon D3200 and 18 mm focal length) the flying altitude can be set to 150 m and achieve the same mapping parameters. Such a setting would allow a photographic footprint of 24,704 m^2 and still provide a GSD of 0.03 m.

8 OUTLOOK

In the current thesis work, a new methodology for estimating snow depth spatial distribution was investigated. With the first results obtained, great potentialities can be foreseen in the method for a future applicability over realistic and commercial case scenarios. However, various issues still need to be addressed, tested and improved. Future work will be aimed at further testing the *co-georeferenciation* procedure. This is considered an extremely important asset for the future applicability of the method that could further improve the achieved accuracies if properly applied. Other investigations have to be done in regards of how to solve the snow depth underestimation in the case of vegetation covered topographies. Furthermore, estimations of volume and SWE derived from snow depth data gathered through this methodology needs to be tested and validated. For example, it would result interesting to apply proposed statistical models able to estimate snow density distribution from snow depth data, snow class type and date of the year for more accurate SWE determinations (Sturm, et al., 2010). Finally, this UAV-borne method also aims to be a tool for extracting precise snow depth data that can be used as input for snow distribution modeling. A similar approach has been previously done using HS data retrieved from airborne LiDAR (Baños, et al., 2011). But, being able economically and repeatdly retrieved this kind of data would represent a huge advantage over these previous studies. Further research in this direction is to be followed.

BIBLIOGRAPHY

Agisoft, 2013. *Agisoft Photoscan User Manual: Professional Edition, Version 1.0.0.* St. Petersburg: s.n.

Akyürek, Z. & Şorman, A. Ü., 2002. Monitoring snow-covered areas using NOAA-AVHRR data in the eastern part of Turkey. *Hydrological Sciences Journal,* 47(2), pp. 243-252.

Al-Wassai, F. A. & Kalyankar, N., 2013. Major Limitations of Satellite images. *Journal of Global Research in Computer Science,* 4(5), pp. 51-59.

Avanzi, F., De Michele, C. & Ghezzi, A., 2014. Liquid-Solid Partitioning of Precipitation along an Altitude Gradient and Its Statistical Properties: An Italian Case Study. *American Journal of Climate Change,* 3(1), pp. 71-82.

Ballabeni, A., Apollonio, F., Gaiani, M. & Remondino, F., 2015. *Advances in image pre-processing to improve automated 3D reconstruction.* Avila, Spain, The International Archives of the Photogrammetry, Remote Sensing and Spatial Information Sciences, pp. 25-27.

Baños, I. et al., 2011. Assessment of airborne LIDAR for snowpack depth. *Boletín de la Sociedad Geológica Mexicana,* Volume 63, pp. 95-107.

Barnett, T. P., Adam, J. C. & Lattenmaier, D., 2005. Potential impacts of a warming climate on water availability in snow-dominated regions. *Nature,* Volume 438, pp. 303-309.

Bavera, D. et al., 2014. A comparison between two statistical and a physically-based model in snow water equivalent mapping. *Advances in Water Resources,* Volume 63, pp. 167-178.

Bøggild, C., Knudby, C., Knudsen, M. & Starzer, W., 1999. Snowmelt and runoff modelling of an Arctic hydrological basin in west Greenland. *Hydrological Processes,* Volume 13, pp. 1989-1990.

Bormann, K., Westra, S., Evans, J. & McCabe, M., 2013. Spatial and temporal variability in seasonal snow density. *Journal of Hydrology,* Volume 484, pp. 63-73.

Bruland, B. et al., 2015. Weather SDM: estimating snow density with high precision using snow depth and local climate. *Hydrology Research,* 46(4), pp. 494-506.

Bruland, O. et al., 2004. Modelling the snow distribution at two high arctic sites at Svalbard, Norway, and at an alpine site in central Norway. *Nordic Hydrology,* 35(3), pp. 191-208.

Bühler, Y. et al., In press. Spatially continuous mapping of snow depth in high alpine catchments using digital photogrammetry. *The Cryosphere.*

Burrough, P. & McDonnell, R., 1998. *Principles of Geographic Information Systems.* New York: Oxford University Press.

Butt, M. & Bilal, M., 2011. Application of snowmelt runoff model for water resource management. *Hydrological Processes,* 25(24), pp. 3735-3747.

Callaghan, T. V. et al., 2011. Multiple Effects of Changes in Arctic Snow Cover. *Ambio,* 40(1), pp. 32-45.

Cimoli, E. & Marcer, M., 2014. *Digital Elevation Model Reconstruction of a Glaciarized Basin Using Land-Based Structure from Motion,* Copenhagen: Arctic Technology Centre.

Clifford, D., 2010. Global estimates of snow water equivalent from passive microwave instruments: history, challenges and future developments. *International Journal of Remote Sensing,* Volume 31, pp. 3707-3726.

Colbeck, S. C., 1982. An overview of seasonal snow metamorphism. *Reviews of Geophysics,* 20(1), pp. 45-61.

Colomina, I. & Molina, A., 2014. Unmanned aerial systems for photogrammetry and remote sensing: A review. *ISPRS Journal of Photogrammetry and Remote Sensing,* Volume 92, pp. 79-97.

Deems, J. S. & Painter, T., 2006. *Lidar Measurement of Snow Depth: Accuracy and Error Sources.* Telluride, Colorado, International Snow Science Workshop Proceedings - Montana State University Library.

Deems, J. S., Painter, T. H. & Finnegan, D. C., 2013. Lidar measurement of snowdepth: a review. *Journal of Glaciology,* 59(215), pp. 467-479.

Dèry, S. & Brown, R. D., 2007. Recent Northern Hemisphere snow cover extent trends and implications for the snow-albedo feedback. *Geophysical Research Letters,* Volume 34, pp. 1-6.

Dietz, A. J., Kuenzer, C., Gessner, U. & Dech, S., 2011. Remote sensing of snow - a review of available methods. *International Journal of Remote Sensing,* 33(13), pp. 4094-4134.

Dowling, T. & Gallant, J. C., 2013. *High Resolution DEMs from Unmanned Aerial Vehicles.* Adelaide, Australia, s.n.

Eckerstorfer, M., 2013. *Snow avalanches in central Svalbard : a field study of meteorological and topographical triggering factors and geomorphological significance,* Longyearbyen: Faculty of Mathematics and Natural Sciences, University of Oslo.

Eckerstorfer, M. & Christiansen, H. H., 2011. The "High Arctic Maritime Snow Climate" in Central Svalbard. *Arctic, Antarctic, and Alpine Research,* 43(1), pp. 11-21.

Elder, K., Dozier, J. & Michaelsen, J., 1991. Snow Accumulation and Distribution in an Alpine Watershed. *Water Resources Research,* 27(7), pp. 1541-1552.

Ellis, C. R., Pomeroy, J. W., Brown, T. & MacDonald, J., 2010. Simulation of snow accumulation and melt in needleleaf forest. *Hydrology and Earth System Sciences,* Volume 14, pp. 925-940.

Fierz, C. et al., 2009. *The International Classification for Seasonal Snow on the Ground,* Paris: IHP-VII Technical Documents in Hydrology N°83, IACS Contribution N°1.

Fohn, P., 1989. Climate Change, Snowcover, and Avalanches. In: *Landscape Ecological Impact of Climatic Change on Alpine Regions.* Lunteren, The Netherlands: Discussion report prepared for the European Conference on Landscape Ecological Impact of Climatic Change , pp. 27-33.

Fonstad, M. A. et al., 2013. Topographic structure from motion: a new development in photogrammetric measurement. *Earth Surface Processes and Landforms,* 38(4), pp. 421-430.

Funaki, M., Hirasawa, N. & Group, A. P., 2008. Outline of a small unmanned aerial vehicle (Ant-Plane) designed for Antarctic research. *Polar Science,* Volume 2, pp. 129-142.

Furukawa, Y., Curless, B., Seitz, M. & Szeliski, R., 2010. *Clustering view for multi-view stereo.* San Francisco, IEEE Conference on Computer Vision and Pattern Recognition, pp. 1434-1441.

Furukawa, Y. & Ponce, J., 2007. *Accurate, dense, and robust multi-view stereopsis.* Minneapolis, IEEE Conference on Computer Vision and Pattern Recognition (CVPR).

Furukawa, Y., Sethi, A., Ponce, J. & Kriegman, D., 2004. Structure and Motion from Images of Smooth Textureless Objects. In: *Computer Vision - ECCV 2004.* Berlin: Springer-Verlag, pp. 287-298.

Ghilani, C. & Wolf, P., 2012. *Elementary Surveying An Introduction to Geomatics.* 13th ed. New Jersey: Pearson Education.

Giuliano, M., 2014. *Cultural Heritage: An example of graphical documentation with automated photogrammetric systems.* Riva del Garda, Italy, The International Archives of the Photogrammetry, Remote Sensing and Spatial Information Sciences.

Grünewald, T., Bühler, Y. & Lehning, M., 2014. Elevation dependency of mountain snow depth. *The Cryosphere,* Volume 8, pp. 2381-2394.

Grünewald, T., Schirmer, M., Mott, R. & Lehning, M., 2010. Spatial and temporal variability of snow depth and ablation rates in a small mountain catchment. *The Cryosphere,* Volume 4, pp. 215-225.

Grünewald, T. et al., 2013. Statistical modelling of the snow depth distribution in open alpine terrain. *Hydrology and Earth System Science,* Volume 17, pp. 3005-3021.

Guidi, G., Gonizzi, S. & Micoli, L., 2014. *Image Pre-Processsing for optimizing automated photogrammetry performances.* Riva del Garda, Italy, ISPRS Annals of the Photogrammetry, Remote Sensing and Spatial Information Sciences.

Hackney, C. & Clayton, A., 2015. British Society for Geomorphology . In: *Geomorphological Techniques.* s.l.:British Society for Geomorphology.

Harwin, S. & Lucieer, A., 2012. *An accuracy assessment of georeferenced point clouds produced via multi-view stereo techniques applied to imagery acquired via unmanned aerial vehicle.* Melbourne, Australia, International Archives of the Photogrammetry, Remote Sensing and Spatial Information Sciences.

Hopkinson, C., Sitar, M., Chasmer, L. & Treitz, P., 2004. Mapping snowpack deep beneath forest canopies using airborne lidar. *Photogrammetric Engineering & Remote Sensing,* 70(3), pp. 323-330.

ISO 15739, 2013. *Photography. Electronic still-picture imaging. Noise measurements,* s.l.: BSI.

Jacobson, R., Ray, S., Attridge, G. & Axford, R., 2000. *The manual of Photography.* Oxford: Reed Educational and Professional Publishing Ltd.

Jain, S., Goswami, A. & Saraf, A., 2008. Accuracy assessment of MODIS, NOAA and IRS data in snow cover mapping under Himalayan conditions. *International Journal of Remote Sensing,* Volume 29, pp. 5863-5878.

James, M. & Robson, S., 2012. Straightforward reconstruction of 3D surfaces and topography with a camera: Accuracy and geoscience application. *Journal of Geophysical Research,* 117(F3).

James, M. & Robson, S., 2014. Mitigating systematic error in topographic modelsderived fr om UAVand gr ound-based image networks. *Earth Surface Processes and Landforms,* Volume 39, pp. 1413-1420.

Jamieson, B. & Stethem, C., 2002. Snow avalanche hazards and management in Canada: challenges and progress. *Natural Hazards,* Volume 26, pp. 35-53.

Jonas, T., Marty, C. & Magnusson, J., 2009. Estimating the snow water equivalent from snow depth measurements in the Swiss Alps. *Journal of Hydrology,* Volume 378, pp. 161-167.

Klos, P., Link, T. & Abatzoglou, J., 2014. Extent of the rain-snow transition zone in the western U.S. under historic and projected climate. *Geophysical Research Letters,* 41(13), pp. 4560-4568.

König, M. & Sturm, M., 1998. Mapping snow distribution in the Alaskan Arctic using aerial photography and topographic relationships. *Water Resources Research,* Volume 34, pp. 3471-3483.

Kontogianni, G., Stathopoulou, E. K., Georgopoulos, A. & Doulamis, A., 2015. *HDR imaging for feature detection on detailed architectural scenes.* Avila, Spain, The International Archives of the Photogrammetry, Remote Sensing and Spatial Information Sciences.

Lee, C. Y., Jones, S. D., Bellman, C. J. & Buxton, L., 2008. Dem creation of a snow covered surface using digital aerial photography. *The International Archives of the Photogrammetry, Remote Sensing and Spatial Information Sciences,* Volume XXXVII-B8, pp. 831-836.

Lehning, M., Löwe, H., Ryser, M. & Raderschall, N., 2008. Inhomogeneous precipitation distribution and snow transport in steep terrain. *Water Resources Research,* 44(7).

Leica Geosystems, n.d. *http://www.surveyequipment.com/.* [Online] Available at: http://www.surveyequipment.com/PDFs/leica-lgo-8.3-online-help.pdf [Accessed 22 March 2015].

Lemke, P. et al., 2007. Observations: change in snow, ice and frozen ground. In: *Climate Change 2007: The Physical Science Basis.* Cambridge: Cambridge University Press, pp. 337-384.

Lisein, J. et al., 2013. Aerial surveys using an Unmanned Aerial System (UAS): comparison of different methods for estimating the surface area of sampling strips. *Tropical Conservation Science,* 6(4), pp. 506-520.

Liston, G. E. & Sturm, M., 2002. Winter precipitation patterns in arctic Alaska determined from a blowing-snow model and snow-depth observations. *Journal of Hydrometeorology,* Volume 3, pp. 646-659.

Liston, G. & Sturm, M., 2002. Winter Precipitation Patterns in Arctic Alaska Determined from a Blowing-Snow Model and Snow-Depth Observations. *Journal of Hydrometeorology,* Volume 3, pp. 646-659.

Li, Z., Zhu, C. & Gold, C., 2005. *Digital Terrain Modeling: Principles and Methodology.* 1th ed. s.l.:CRC Press.

López-Moreno, J. et al., 2013. Small scale spatial variability of snow density and depth over complex alpine terrain: Implications for estimating snow water equivalent. *Advances in Water Resources,* Volume 55, pp. 40-52.

Lowe, D., 2004. Distinctive Image Features from Scale-Invariant Keypoints. *Journal of Computer Vision,* 60(2), pp. 91-100.

Lucieer, A. et al., 2012. Using a micro-UAV for ultra-high resolution multisensor observations of Antarctic moss beds. *International Archives of the Photogrammetry,* Volume XXXIX-B1, pp. 429-433.

Lucieer, A. et al., 2012. Using a micro-UAV for ultra-high resolution multi-sensor observations of Antarctic moss beds. *The International Archives of the Photogrammetry, Remote Sensing and Spatial Information Sciences,* Volume XXXIX-B1, pp. 429-433.

Machguth, H., Eisen, O., Paul, F. & Hoezle, M., 2006. Strong spatial variability of snow accumulation observed with helicopter-borne GPR on two adjacent Alpine glaciers. *Geophysical Research Letters,* 33(13), pp. 1-5.

Mancini, M. et al., 2013. Using Unmanned Aerial Vehicles (UAV) for High-Resolution Reconstruction of Topography: The Structure from Motion Approach on Coastal Environments. *Remote Sensing,* Volume 5, pp. 6880-6898.

Marsh, C., Pomeroy, W. & Spiteri, R., 2012. Implications of mountain shading on calculating energy for snowmelt using unstructured triangular meshes. *Hydrological Processes,* 26(12), pp. 1767-1778.

McCreight, J. L. & Small, E. E., 2014. Modeling bulk density and snow water equivalent using daily snow depth observations. *The Cryosphere,* Volume 8, pp. 521-536.

McKay, G., 1968. *Problems of measuring and evaluating snow cover.* Ottawa, Secretariat Canadian National Committee for the IHD.

Micheletti, N., Chandler, J. H. & Lane, S., 2015. Structure from Motion (SfM) Photogrammetry. In: *Geomorphological Techniques.* s.l.:British Society for Geomorphology.

Nolan, M., Larsen, C. & Sturm, M., 2015. Mapping snow depth from manned aircraft on landscape scales at centimeter resolution using structure-from-motion photogrammetry. *The Cryosphere,* Volume 9, pp. 1445-1463.

Parajka, J. & Blöschl, G., 2008. Spatio-temporal combination of MODIS images – potential for snow cover mapping. *Water Resources Research,* Volume 44, pp. 1-13.

Peng, S., Piao, S., Ciais, P. & Fang, J., 2010. Change in winter snow depth and its impacts on vegetation in China. *Global Change Biology,* Volume 16, pp. 3004-3013.

Prokop, A., 2008. Assessing the applicability of terrestrial laser scanning for spatial snow depth measurements. *Cold Regions Science and Technology,* 54(3), pp. 155-163.

Prokop, A. et al., 2008. A comparison of measurement methods: terrestrial laser scanning, tachymetry and snow probing for the determination of the spatial snow-depth distribution on slopes. *Annals of Glaciology,* Volume 49, pp. 210-216.

Remondino, F. & El-Hakim, S., 2006. Image-Based 3D Modeling: A Review. *The Photogrammetric Record Journal,* Volume 21, pp. 269-291.

Rittger, K., Painter, T. & Dozier, J., 2013. Assessment of methods for mapping snow cover from MODIS. *Advances in Water Resources,* Volume 51, pp. 367-380.

Robinson, D. A., Dewey, K. F. & Heim Jr, R. R., 1993. Global snow cover monitoring: an update. *Bulletin of the American Meteorological Society ,* pp. 1689-1696.

Rott, H. et al., 2008. CoReH2O - A Ku- and X-Band SAR Mission for Snow and Ice Monitoring. *IEEE International Journal Geoscience and Remote Sensing,* Volume 47, pp. 3347-3364.

Ryan, J. et al., 2015. UAV photogrammetry and structure from motion to assess calving dynamics at Store Glacier, a large outlet draining the Greenland ice sheet. *The Cryosphere,* Volume 9, pp. 1-11.

Schewe, J. & Fraser, B., 2010. *Real World Image Sharpening with Adobe Photoshop, Camera Raw, and Lightroom.* 2nd ed. Berkeley: Peachpit Press.

Schweizer, J., Kronholm, K., Jamieson, J. & Birkeland, K., 2008. Review of spatial variability of snowpack properties and its importance for avalanche formation. *Cold Regions Science and Technology,* 51(2-3), pp. 253-272.

Scipiòn, D. et al., 2013. Seasonal small-scale spatial variability in alpine snowfall and snow accumulation. *Water Resources Research,* Volume 49, pp. 1446-1457.

Serreze, M. C. et al., 1999. Charcteristics of the western United States snowpack from snowpack telemetry (SNOTEL) data. *Water Resources Research,* 35(7), pp. 2145-2160.

Slater, A. & Clark, M. P., 2006. Snow data assimilation via ensemble Kalman filter. *Journal of Hydrometeorology,* Volume 7, pp. 478-493.

Snavely, N., 2008. *Scene reconstruction and visualization from internet photo collections,* USA: s.n.

Solbø, S. & Storvold, R., 2013. *Mapping Svalbard glaciers with the cryowing UAS.* Rostock, Germany, International Archives of the Photogrammetry, Remote Sensing and Spatial Information Sciences.

Sommerfeld, R. A. & Lachapelle, E., 1970. The classification of snow metamorphism. *Journal of Glaciology,* 9(55), pp. 3-17.

Street, R. & Melnikov, P., 1990. Seasonal snow cover, ice and permafrost. In: I. Press, ed. *Climate Change: The IPCC Impacts Assesment.* Canberra, Australia: Australian Government Publishing Service, pp. 7-1-7-33.

Sturm, M., Holmgren, J. & Liston, G., 1994. A seasonal Snow Cover Classification System for Local to Global Applications. *American Meteorological Society,* pp. 1261-1283.

Sturm, M. et al., 2010. Estimating Snow Water Equivalent Using Snow Depth Data and Climate Classes. *Journal of Hydrometeorology,* Volume 11, pp. 1380-1394.

Taylor, J., 1997. *An Introduction to Error Analysis: The Study of Uncertainities in Physical Measurements.* s.l.:University Science Books.

Triggs, B., McLauchlan, P., Hartley, R. & Fitzgibbon, A., 1999. *Bundle Adjustment - A Modern Synthesis.* Corfu, Greece, Springer-Verlag, pp. 298-372.

Turner, D., Lucieer, A. & Watson, C., 2014. Direct Georeferencing of Ultrahigh-Resolution UAV Imagery. *Geoscience and Remote Sensing ,* 25(5), pp. 2735-2745.

U.N. Office for Outer Space Affairs, 2012. *Education Curriculum Global Navigation Satellite Systems,* New York: Publishing and Library Section, United Nations Office at Vienna.

UNEP, 2007. *Global Outlook for Ice and Snow,* Arendal, Norway: UNEP/GRID.

Uren, J. & Price, W., 2010. *Surveying for Engineers.* 5th ed. Houndmills: Palgrave Macmillan.

Vikhamar, D. & Solberg, R., 2003. Snow-cover mapping in forests by constrained linear spectral unmixing of MODIS data. *Remote Sensing of Environment,* Volume 88, pp. 309-323.

Wanga, K. et al., 2013. Snow effects on alpine vegetation in the Qinghai-Tibetan Plateau. *International Journal of Digital Earth,* 8(1), pp. 56-73.

Wechsler, S., 2007. Uncertainties associated with digital elevation models for hydrologic applications: a review. *Hydrology and Earth System Sciences,* Volume 11, pp. 1481-1500.

Wechsler, S. P. & Kroll, C., 2006. Quantifying DEM Uncertainty and its Effect on Topographic Parameters. *Photogrammetric Engineering & Remote Sensing,* Volume 72, p. 1081–1090.

Westoby, M., Brasington, J., Glasser, N. & Hambrey, M., 2012. 'Structure-from-Motion' photogrammetry: A low-cost, effective tool for geoscience applications'. *Geomorphology,* Volume 179, pp. 300-314.

Winther, J. G. et al., 2003. Snow Research in Svalbard-an overview. *Polar Research,* 22(2), pp. 125-144.

Wolf, P., Dewitt, B. A. & Wilkinson, B., 2014. *Elements of Photogrammetry with Applications in GIS, Fourth Edition.* 4th ed. s.l.:McGraw-Hill Education.

Worby, A. P. et al., 2008. Evaluation of AMSRE snow depth product over East Antarctic sea ice using in situ measurements and aerial photography. *Journal of Geophysical Research,* 113(C5).

Xhardè, R., Long, B. & Forbes, D., 2006. *Accuracy and Limitations of Airborne LiDAR Surveys in Coastal Environments.* Denver, Geoscience and Remote Sensing Symposium, 2006. IGARSS 2006. IEEE International Conference, pp. 2412-2415.

9 APPENDICES

9.1 APPENDIX 1: SNOW SURFACES AND UNDERLYING TOPOGRAPHIES ORTHOPHOTOS ALONG WITH USED GCPS POSITIONS

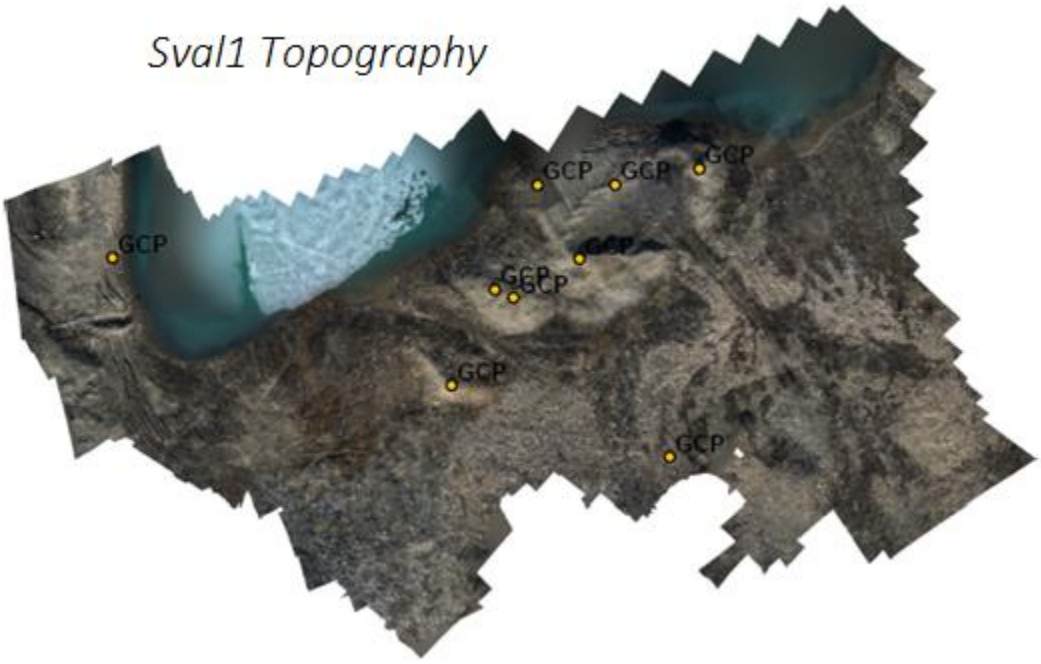

Sval2 Snow Surface

Sval2 Topography

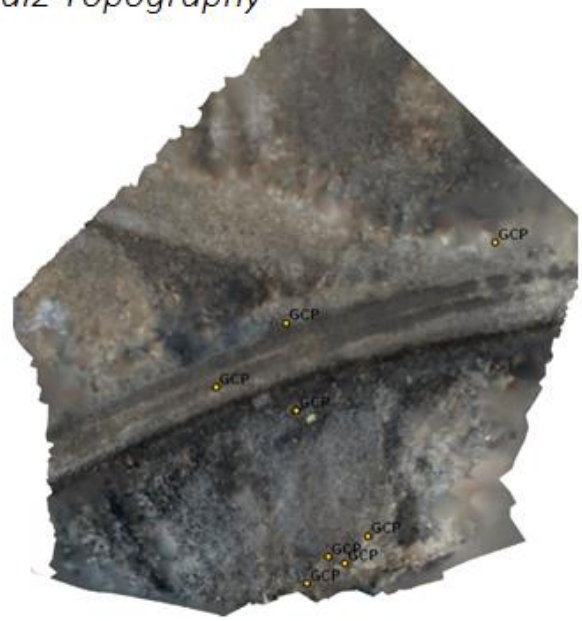

Green1 Snow Surface

Green1 Topography

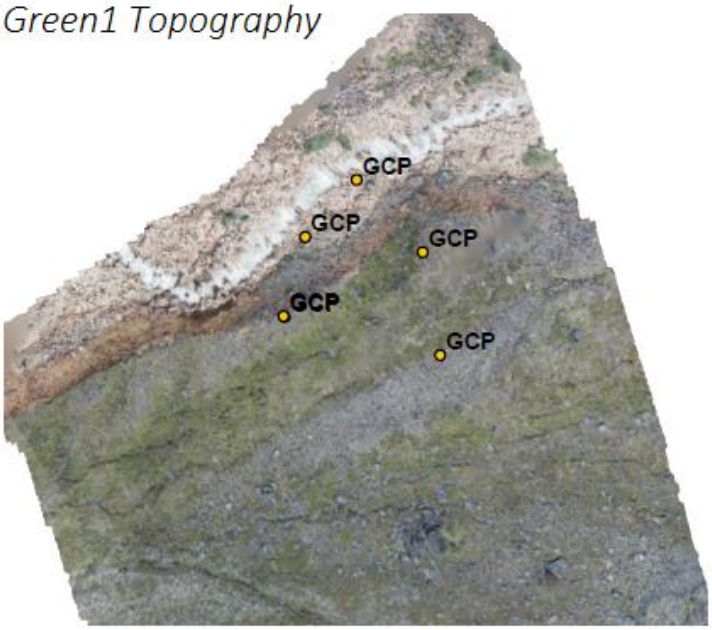

Green2 Snow Surface

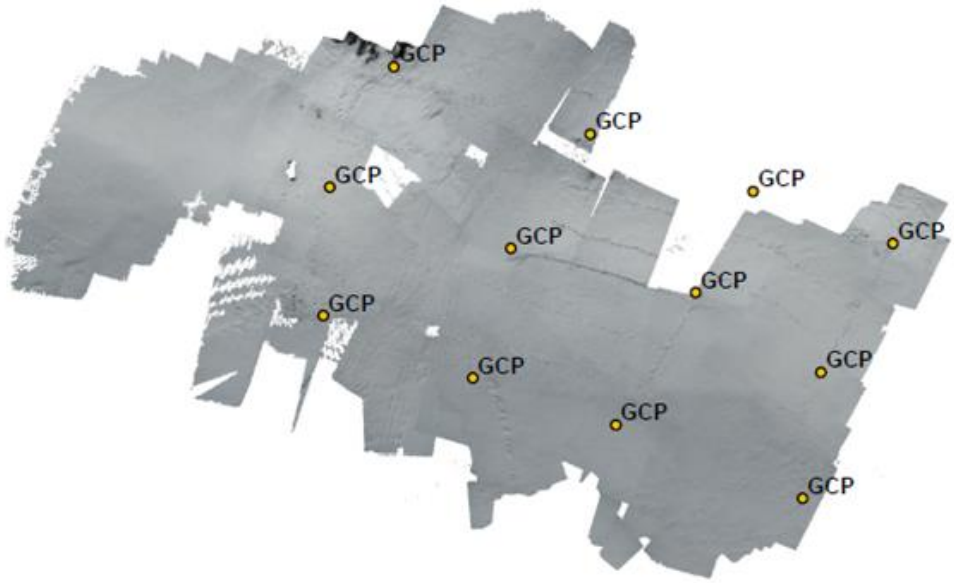

Green2 Topography

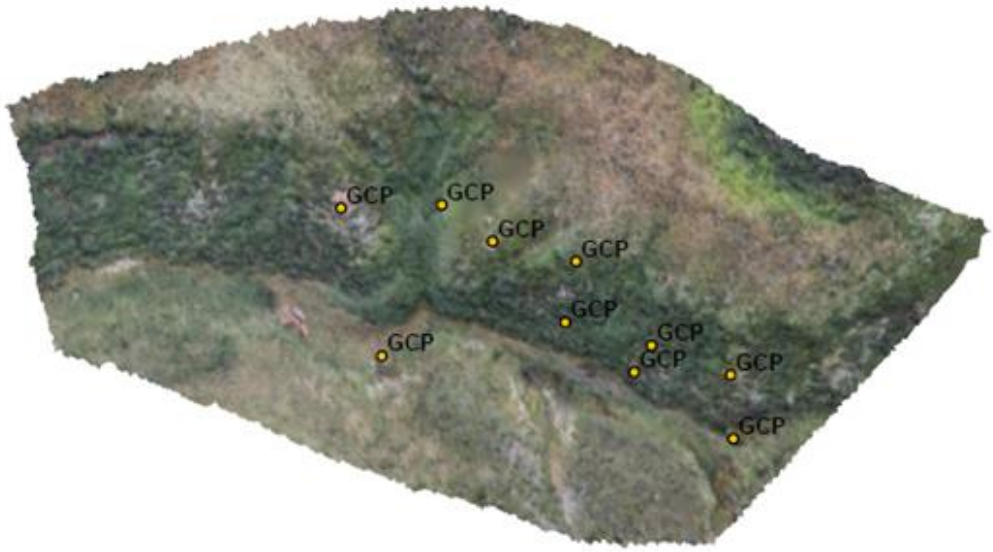

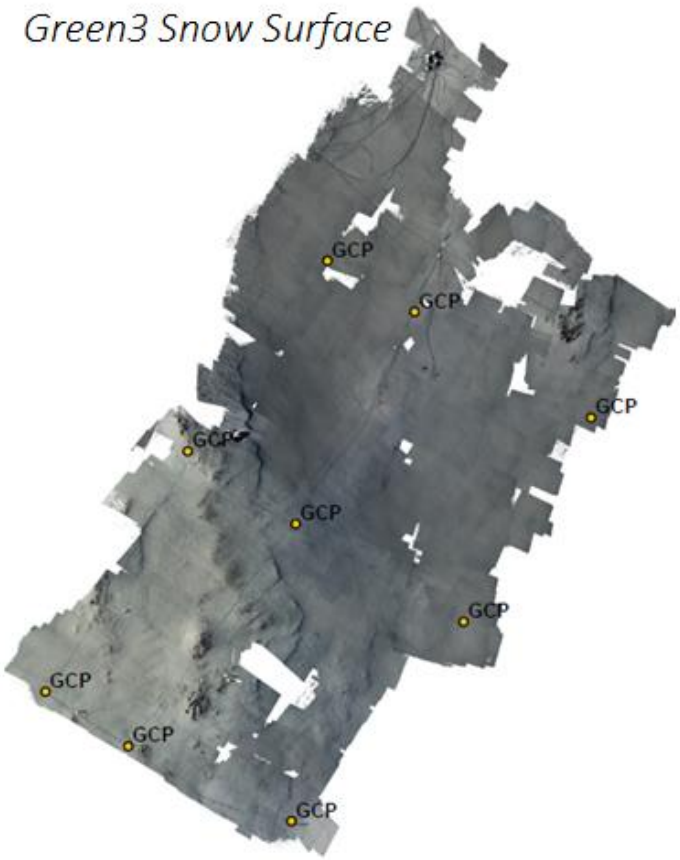
Green3 Snow Surface
GCP
GCP
GCP
GCP
GCP
GCP
GCP
GCP
GCP

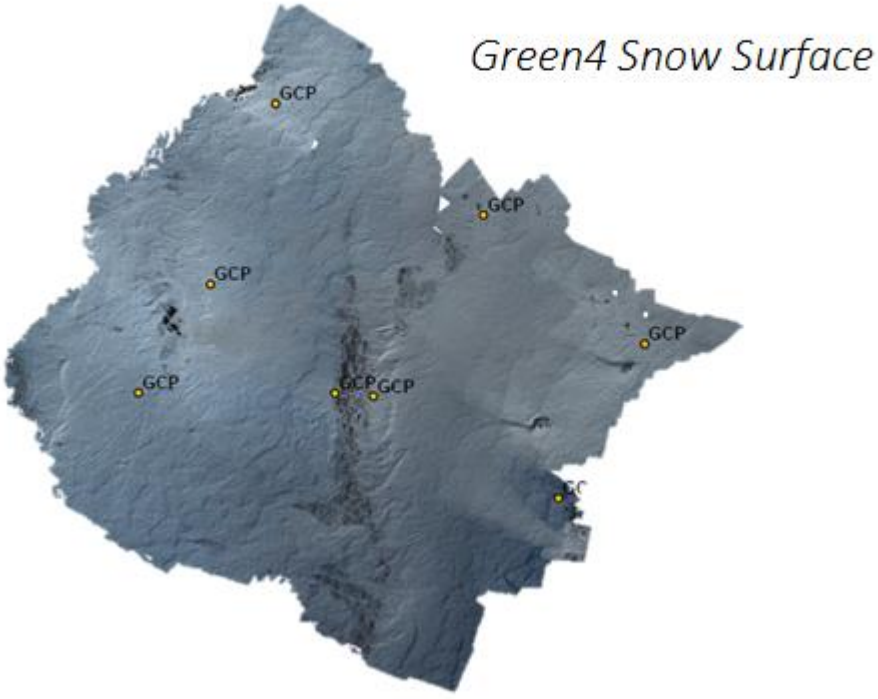
Green4 Snow Surface
GCP
GCP
GCP
GCP
GCP
GCP
GCP

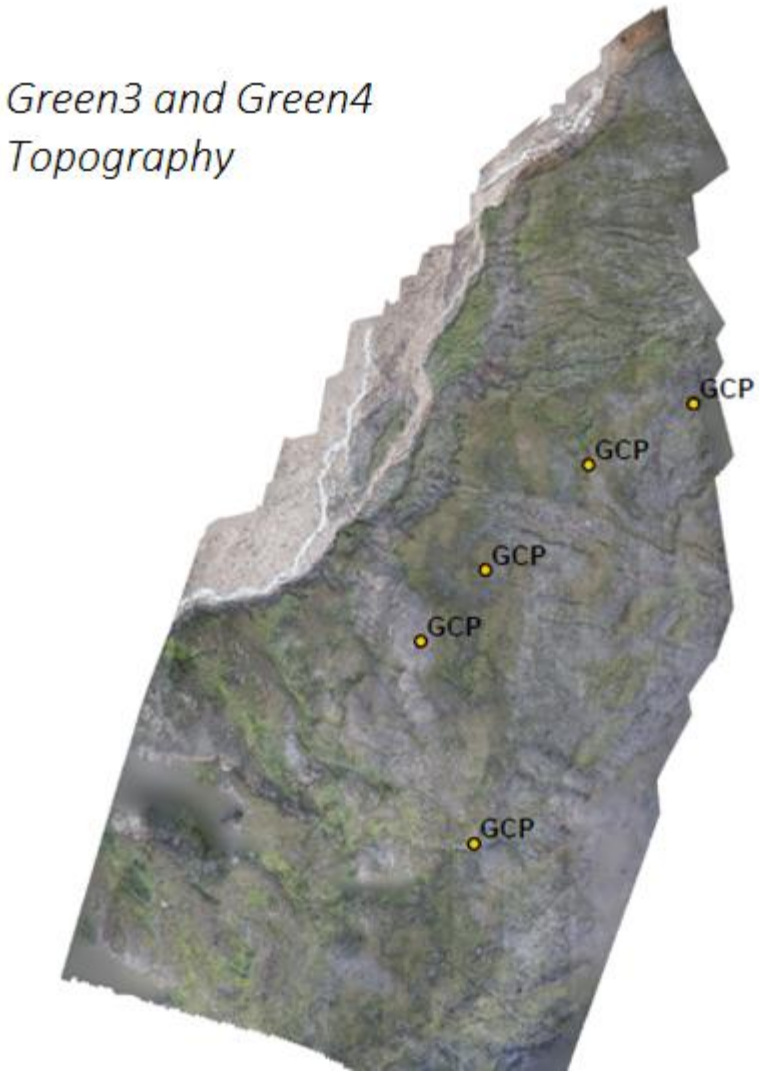
Green3 and Green4
Topography
GCP
GCP
GCP
GCP
GCP

9.2 Appendix 2: Winter UAV flight routes, camera positions and Image overlap from Sval1 to Green4 respectively

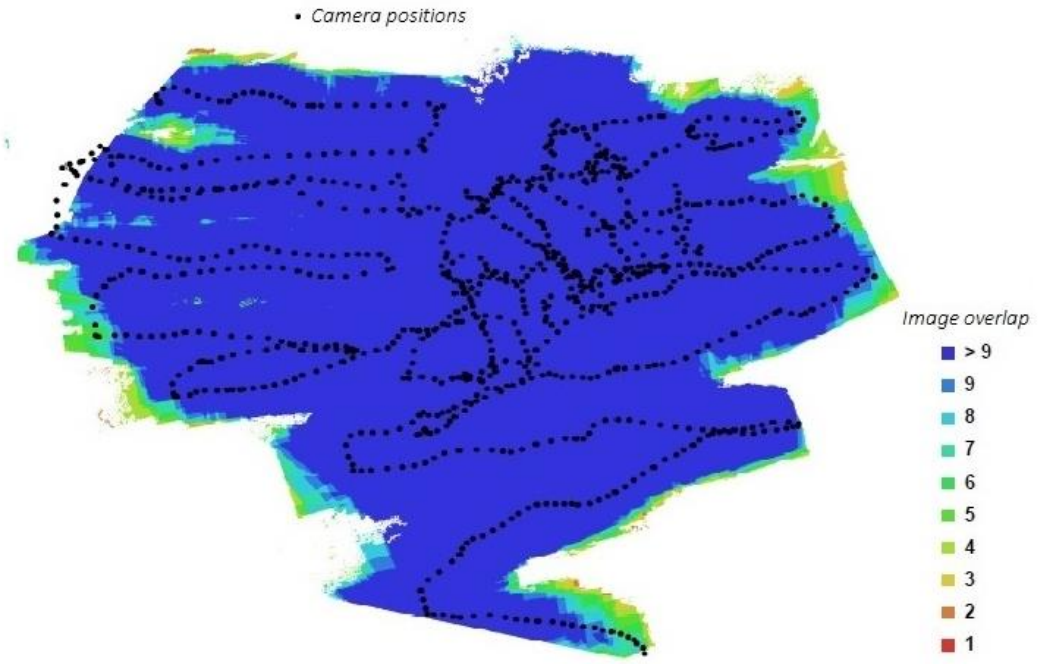

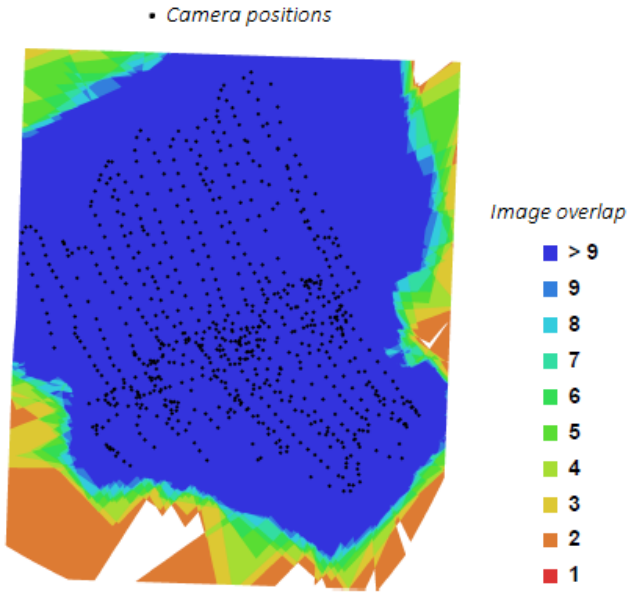

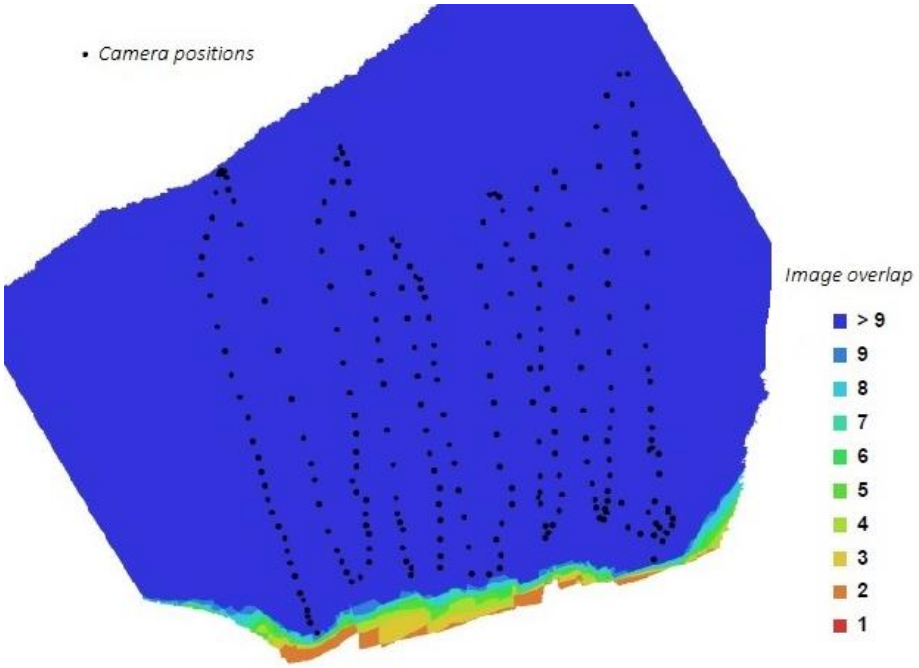
• Camera positions
Image overlap
> 9
9
8
7
6
5
4
3
2
1

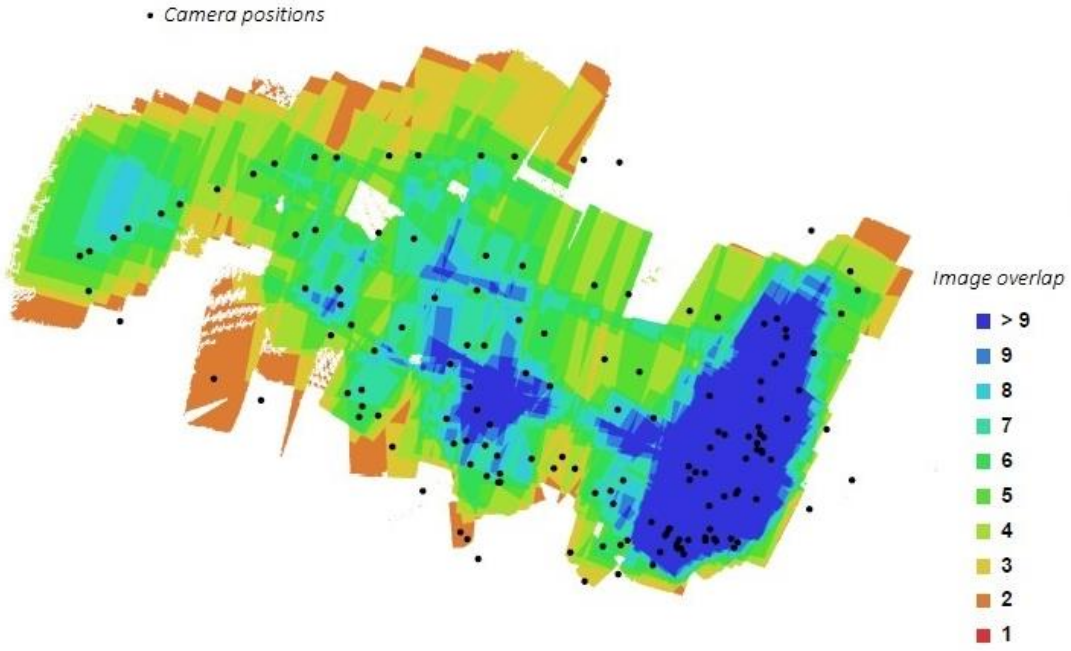
• Camera positions
Image overlap
> 9
9
8
7
6
5
4
3
2
1

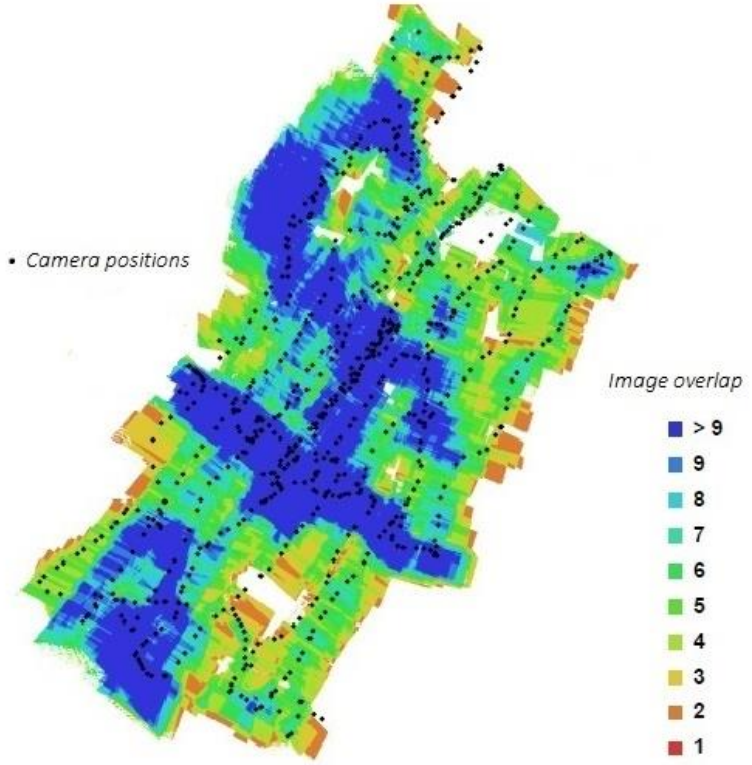
• Camera positions
Image overlap
> 9
9
8
7
6
5
4
3
2
1

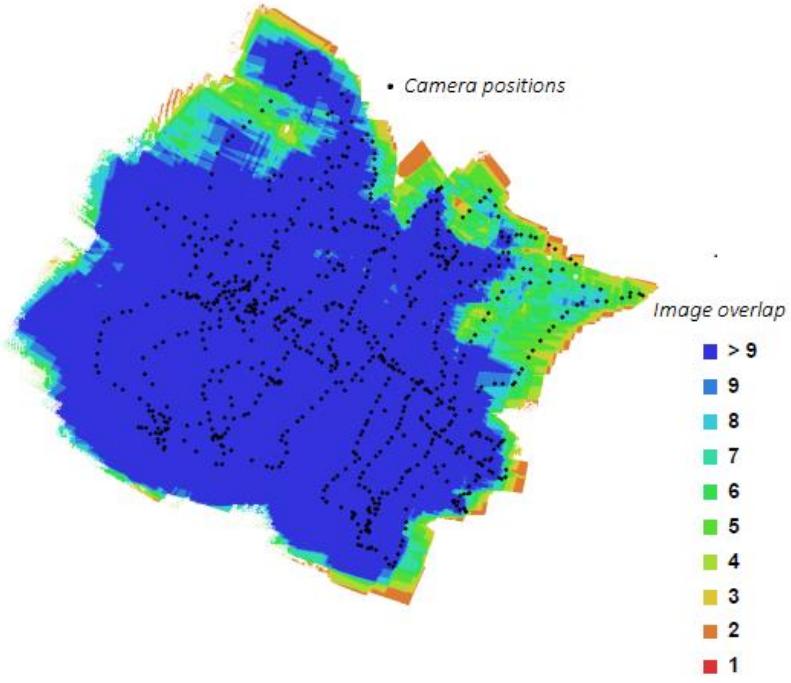
• Camera positions
Image overlap
> 9
9
8
7
6
5
4
3
2
1

9.3 APPENDIX 3: MATLAB SCRIPT FOR SNOW DEPTH ESTIMATION

```
%% Import Snow Surface

[RGB1, R1, bbox1] = geotiffread('Snow.tif');
[s11 s12]=size(RGB1);
for i=1:s11
     h=ones(1,s12);
[x1(i,:),y1(i,:)] = pix2map(R1,h*i,1:s12);
end

%% Import Topography

[RGB2, R2, bbox2] = geotiffread('Topo.tif');
[p11 p12]=size(RGB2);
for i=1:p11
     f=ones(1,p12);
[x2(i,:),y2(i,:)] = pix2map(R2,f*i,1:p12);
end

%% Align and interpolates snow DEM and topogrpahy DEM

RGB2_int=interp2(x2,y2,RGB2,x1,y1);

%% Performs Subtraction and snow error filtering

clear a b
[a b]=find(abs(RGB1)>3);
for i=1:size(a,1)
    HS(a(i),b(i))=0;
end

HS=zeros(size(RGB1,1),size(RGB1,2));
for i=1:size(RGB1,1)
    for j=1:size(RGB1,2)
        if RGB1(i,j)==0 || RGB2_int(i,j)==0
            HS(i,j)==0;
        else
            HS(i,j)=RGB1(i,j)-RGB2_int(i,j);
        end
        if HS(i,j)>5
            HS(i,j)=5;
        end
        if HS(i,j)<-2
            HS(i,j)=-2;
        end
    end
end
contourf(x1,y1,HS);

%% Clean Snow Depth Map

HS(isnan(HS)) = 0 ;
```

```
HS( HS==5 )=0;
HS( HS==-2 )=0;


%% Displays Map

HS( HS==0 )=NaN;

imagesc(HS);
title('Snow Depth Distribution Map')

%% Generates snow depth geotiff file in the same coordinate system

info = geotiffinfo('Snow.tif');
geotiffwrite('SnowDepth.tif', HS, R1, ...
 'GeoKeyDirectoryTag', info.GeoTIFFTags.GeoKeyDirectoryTag);
```

9.4 Appendix 4: Image Pre-processing findings

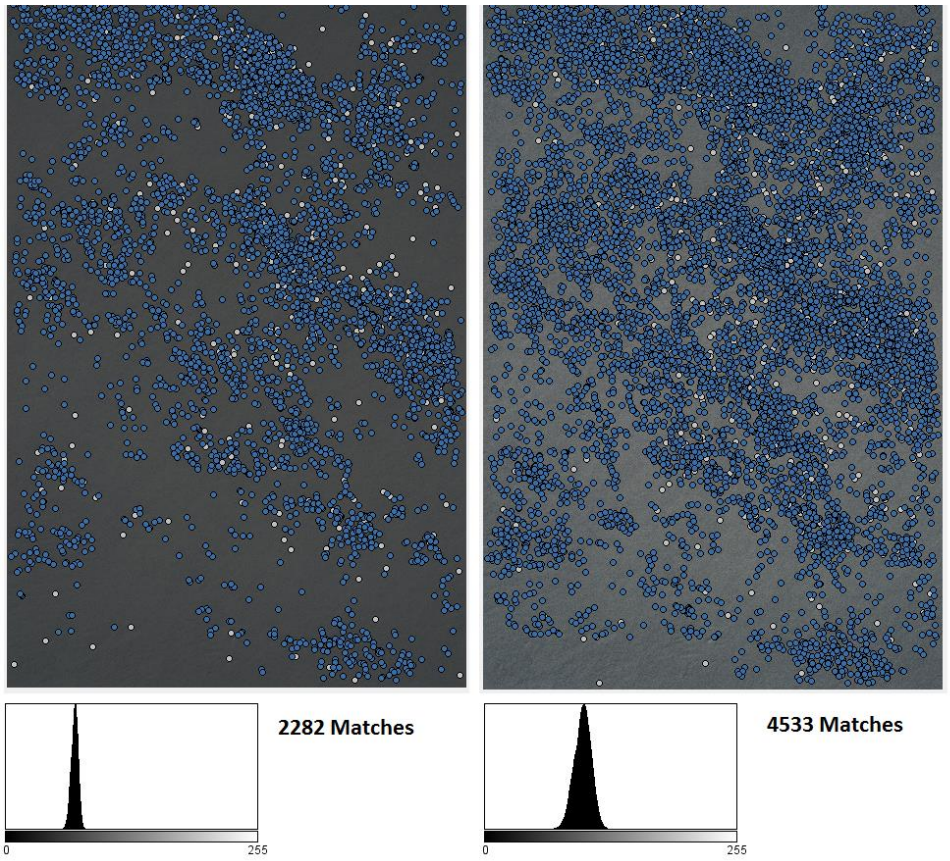

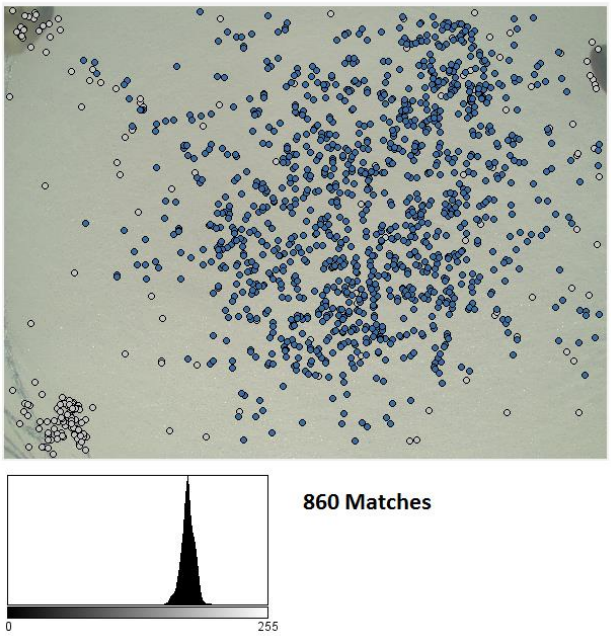
0
255
860 Matches
0
255
1046 Matches

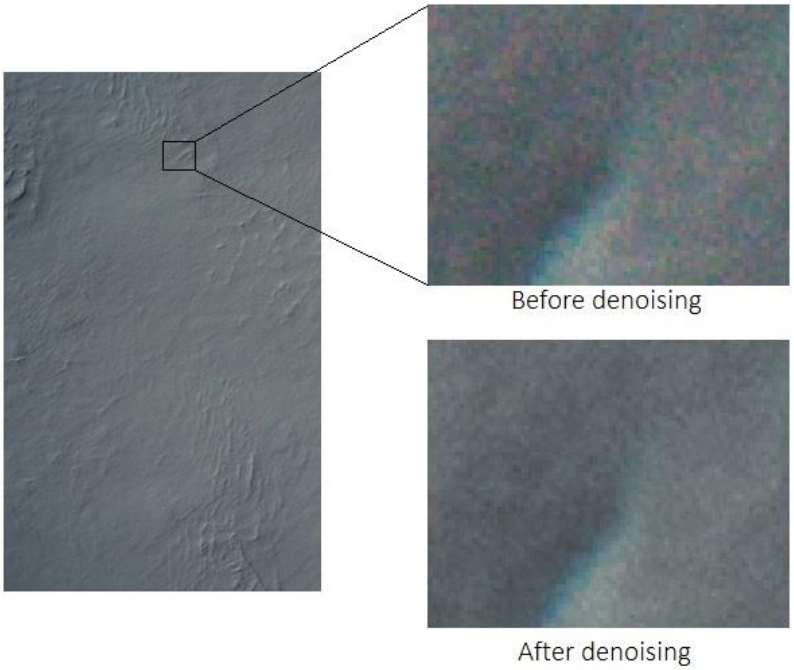
Before denoising
After denoising

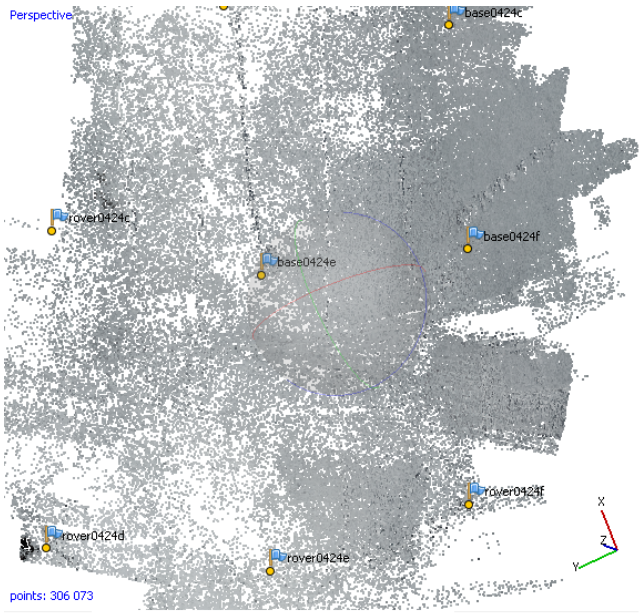

Green2 with pre-processing

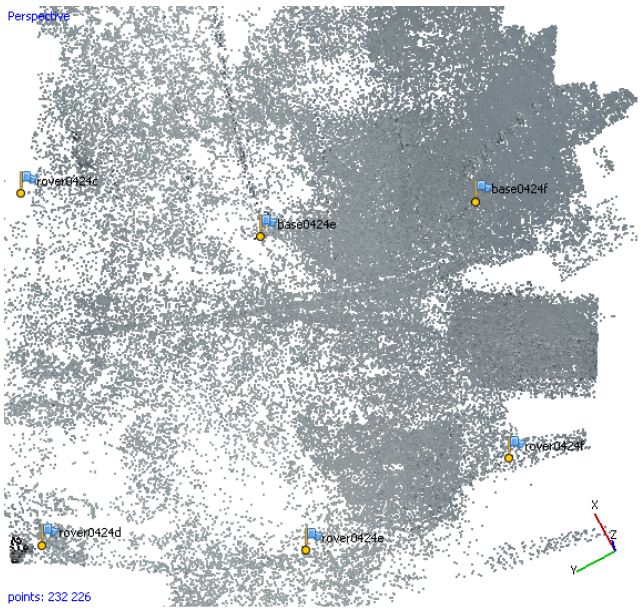

Green2 without pre-processing